Open Access

# Long-Term Lunar Atmospheric Tides in the Southern Hemisphere

Ian R. G. Wilson[1] and Nikolay S. Sidorenkov[*,2]

[1]*The Liverpool Plains Daytime Astronomy Centre, Curlewis, NSW, Australia*

[2]*Hydrometcenter of Russia, Bolshoy Predtechensky 11-13, 123242 Moscow, Russian Federation, Russia*

**Abstract:** The longitudinal shift-and-add method is used to show that there are N=4 standing wave-like patterns in the summer (DJF) mean sea level pressure (MSLP) and sea-surface temperature (SST) anomaly maps of the Southern Hemisphere between 1947 and 1994. The patterns in the MSLP anomaly maps circumnavigate the Earth in 36, 18, and 9 years. This indicates that they are associated with the long-term lunar atmospheric tides that are either being driven by the 18.0 year Saros cycle or the 18.6 year lunar Draconic cycle. In contrast, the N=4 standing wave-like patterns in the SST anomaly maps circumnavigate the Earth once every 36, 18 and 9 years between 1947 and 1970 but then start circumnavigating the Earth once every 20.6 or 10.3 years between 1971 and 1994. The latter circumnavigation times indicate that they are being driven by the lunar Perigee-Syzygy tidal cycle. It is proposed that the different drift rates for the patterns seen in the MSLP and SST anomaly maps between 1971 and 1994 are the result of a reinforcement of the lunar Draconic cycle by the lunar Perigee-Syzygy cycle at the time of Perihelion. It is claimed that this reinforcement is part of a 31/62/93/186 year lunar tidal cycle that produces variations on time scales of 9.3 and 93 years. Finally, an N=4 standing wave-like pattern in the MSLP that circumnavigates the Southern Hemisphere every 18.6 years will naturally produce large extended regions of abnormal atmospheric pressure passing over the semi-permanent South Pacific sub-tropical high roughly once every ~ 4.5 years. These moving regions of higher/lower than normal atmospheric pressure will increase/decrease the MSLP of this semi-permanent high pressure system, temporarily increasing/reducing the strength of the East-Pacific trade winds. This may led to conditions that preferentially favor the onset of La Nina/El Nino events.

**Keywords:** Lunar atmospheric tides, atmospheric pressure, sea-surface temperatures, ENSO, El Nino, La Nina.

## 1. INTRODUCTION

Sidorenkov [1] has determined that the frequency spectra of the ENSO indices has significant components that are close to the sub−harmonics of the free nutation period of the Earth's poles (i.e. the Chandler Wobble) and the super-harmonics of the Earth's forced nutation motion (i.e. the 18.6 year lunar nodical wobble). Sidorenkov [1] argues that external forcing by the lunar/solar tides, acting at the super-harmonics of the Earth's forced nutation motion, could produce non−linear enhancements of the oscillations in the Earth−Atmosphere−Ocean system that closely match those that are seen in the ENSO climate variations. He also asserts that the resultant ENSO climate variations excite the Chandler Wobble through a resonant coupling with the sub−harmonics of the free nutation period of the Earth's pole.

Following on from the work of Sidorenkov [1-4], Li [5], Li and Zong [6], Li *et al.* [7] have shown that cyclical changes in lunar tidal forcing produce atmospheric tides with periods of 27.3 day and 13.6 days. Li and his associates have detected these atmospheric tides in the tropical troposphere at heights above the 700 hPa isobaric surface (~ 3000m). They also indicate that the tides are likely to be present in the upper parts of the mid-latitude troposphere, as well.

Support for the findings of Li *et al.* [7] is provided by Krahenbuhl *et al.* [8] who have shown that the 27.3 day lunar atmospheric tides can influence the short-term mid-latitude general circulation pattern by deforming the high-latitude Rossby long-waves. They also find that these tidal effects have their greatest influence in the upper troposphere of both hemispheres.

Wilson [9] has extended the work of Li *et al.* [7] by showing that the lunar atmospheric tides have an influence upon regional climate variables on inter-annual to decadal time scales. Wilson [9] has shown that variations in the peak latitude anomaly of the summer (DJF) subtropical high pressure ridge over Eastern Australia ($L_{SA}$) exhibits the same period and phase as that of the 18.6/ 9.3 year draconic spring tides.

One obvious way to extend the work of Wilson [9] is to look for evidence of the global effects of these 18.6/9.3 year draconic lunar atmospheric tides upon the general atmospheric circulation patterns of the Southern Hemisphere. One indication that changes in the general circulation pattern of this nature are in fact taking place is the appearance of large-scale periodic patterns in the mean sea-level pressure (MSLP) and sea-surface temperature (SST) anomalies maps of the Southern Hemisphere that vary on time scales of roughly nine years. An example of this type of phenomenon can be seen in Fig. (**1a-c**).

*Address correspondence to this author at the Hydrometcenter of Russian Federation, Bolshoy Predtechensky 11-13, 123242 Moscow, Russia;
Tel: +7(499) 252-34-48; Fax: +7(499) 255-15-82;
E-mail: sidorenkov@mecom.ru

Fig. (**1a**) shows the NOAA SST anomaly map for the 25$^{th}$ of January 1981 (NOAA [10]). Clearly visible in this figure is a longitudinal pattern of four large regions with warmer-than-normal SST that are separated from each other by regions with cooler-than-normal SST. The resultant zonal pattern in the SST anomalies forms an N=4 longitudinal standing wave-like pattern (hereafter referred to as the N=4 pattern) that straddle the Earth's southern oceans between the latitudes 30° and 50° S.

Fig. (**1b**) shows a map of the MSLP anomalies for the Southern Hemisphere north of 60° S, averaged over the Southern summer months (DJF) of 1980 – 81. The MSLP anomalies used in Fig. (**1b**) are those published by the UK Met Office Hadley-Centre (UKMO) in the hadSLP2.asc data set (Adam and Ansell [11]). These anomalies are displayed in 5° × 5° bins of latitude and longitude and they are calculated using the mean monthly MSLP values for the period from 1971 to 2000. Fig. (**1b**) is designed to highlight the seasonal
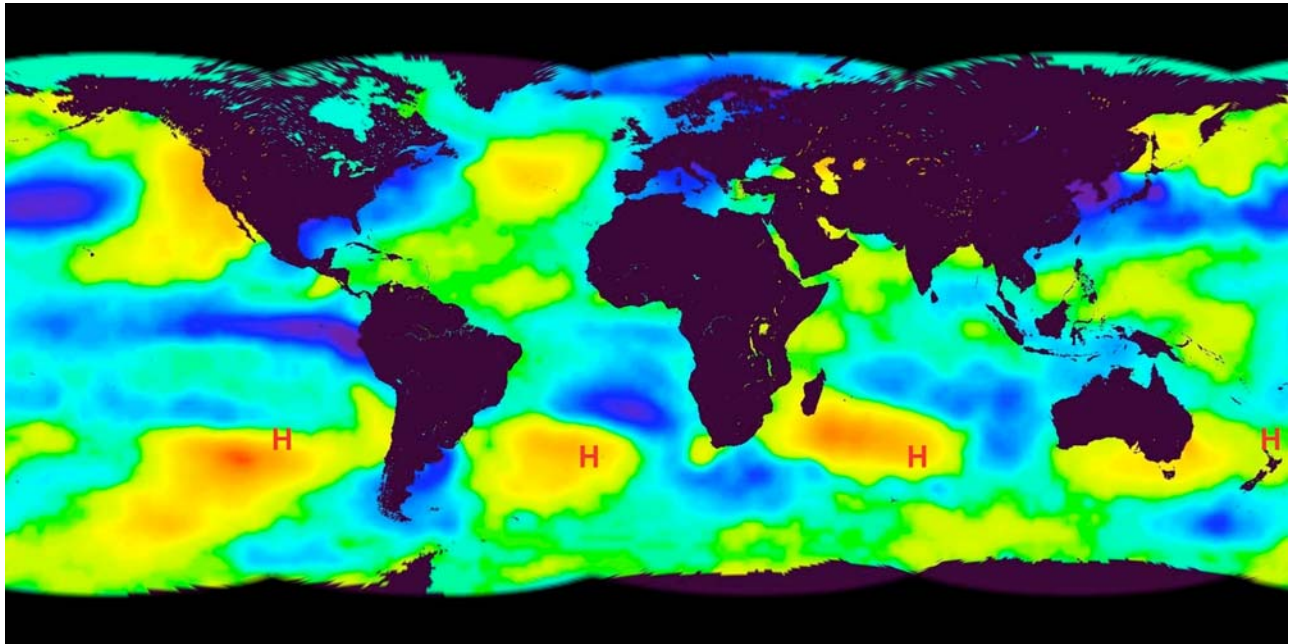


**Fig. (1a).** The NOAA SST anomaly map for the 25$^{th}$ of January 1981.
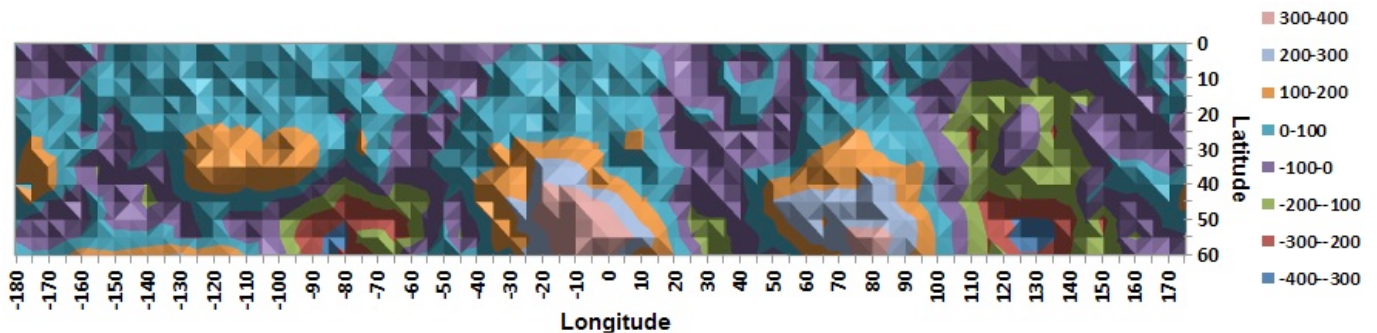


**Fig. (1b).** A map of the MSLP anomalies for the Southern Hemisphere north of 60° S, averaged over the Southern summer months (DJF) of 1980 – 81. This figure is designed to highlight the seasonal MSLP anomalies that were in place over the summer that includes the NOAA SST anomaly map for the 25$^{th}$ of January 1981. The units used for MSLP in this paper are 1/100$^{th}$ hPa, unless noted otherwise.
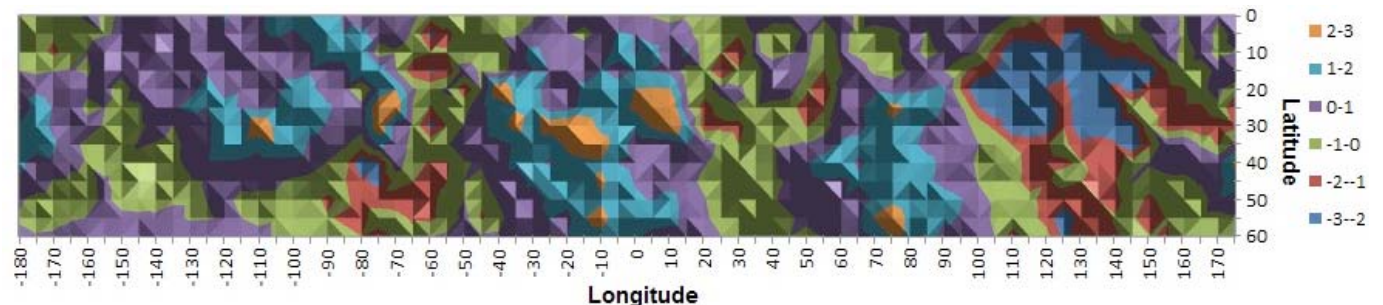


**Fig. (1c).** An equivalent map to that shown in Fig. (**1b**), except that in this map the MSLP anomaly for each 5° × 5° bin has been divided by the value of its standard deviation to show the standardized MSLP anomalies for the Southern Hemisphere north of 60° S.

MSLP anomalies that were in place over the summer that includes the NOAA SST anomaly map for the 25th of January 1981.

Fig. (**1c**) shows an equivalent map to that shown in Fig. (**1b**), except that in this map the MSLP anomaly for each 5° × 5° bin has been divided by the value of its standard deviation to show the standardized MSLP anomalies for the Southern Hemisphere north of 60° S.

[N.B. Normally standardized anomalies are used rather than simple anomalies because they remove the effects of regional and temporal changes in the quality of the data. Unfortunately, there are a considerable number of the standard deviation values missing in the MSLP data, particularly south of 45° S. Hence, this paper will use simple anomalies rather than standardized anomalies because of the concerns about the effects that a high number of missing standard deviation values has upon the quality of the data. This means that (with the exception of Fig. **1c**) all use of standardized anomalies will be restricted to the Appendix **B** where they will be employed to estimate the level of significance of our final results].

Fig. (**1b**) shows that during the southern summer of 1980 – 81, there were four regions of higher-than-normal pressure centred at (35° S, 115° W), (47° S, 15° W), (52° S, 85° E) and (43° S, 170° W). The first three high pressure regions are located in the south-eastern sectors of the Pacific, Atlantic and Indian Oceans, while the last region is roughly centered on the South Island of New Zealand. The location of these high pressure cells closely match the coordinates of the positions of the four semi-permanent high pressure systems that are embedded in the Southern Sub-Tropical High Pressure Ridge (Arhens [12]).

[N.B. A comparison between Fig. (**1b**, **c**) shows the effect of dividing each 5° × 5° data cell by its standard deviation. The first thing to note is that each of the four geographically extended areas of higher-than-normal pressure is statistically significant (See Appendix **B** for a detailed discussion of the data that defends this claim]. The second is that the centres of extended atmospheric feature move northward by about ~ 5° to 10° in latitude, if the standardized MSLP anomalies are used rather than simple MSLP anomalies. The primary reason for the movement of these extended features from south to north is the rapid increase of the measurement uncertainties with increasing latitude, particularly south of 30° S].

The approximate positions of the centres of the four regions of higher-than-normal MSLPs seen in Fig. (**1c**) have been superimposed upon Fig. (**1a**) using the letter "H". This superposition allows us to compare the relative locations of the centres of the four known semi-permanent high pressure systems with the positions of the enhanced SST anomalies. The comparison shows that the spatially extended regions of increased SST anomalies appear on the western sides of these four high pressure systems, producing N=4 pattern in the SSTs that straddle the Earth's southern oceans.

One possible explanation for the temporary appearance of an N=4 pattern in the SST anomalies during the southern summer of 1980/81 is that the semi-permanent high pressure systems in the Southern Hemisphere are periodically enhanced by a longitudinally propagating N=4 standing wave-like pattern in the summer MSLP anomalies. If this is indeed the case, then the temporary increase in the MSLPs of these four high pressure systems would naturally lead to enhanced warm northerly winds on their western sides that would produce regions of warmer-than-normal SSTs. Similarly, the cooler southerly winds on their eastern sides would produce regions of cooler-than-normal SSTs.

Evidence supporting this explanation is provided by Fig. (**2a**, **b**). Fig. (**2a**) shows the average MSLP anomaly between
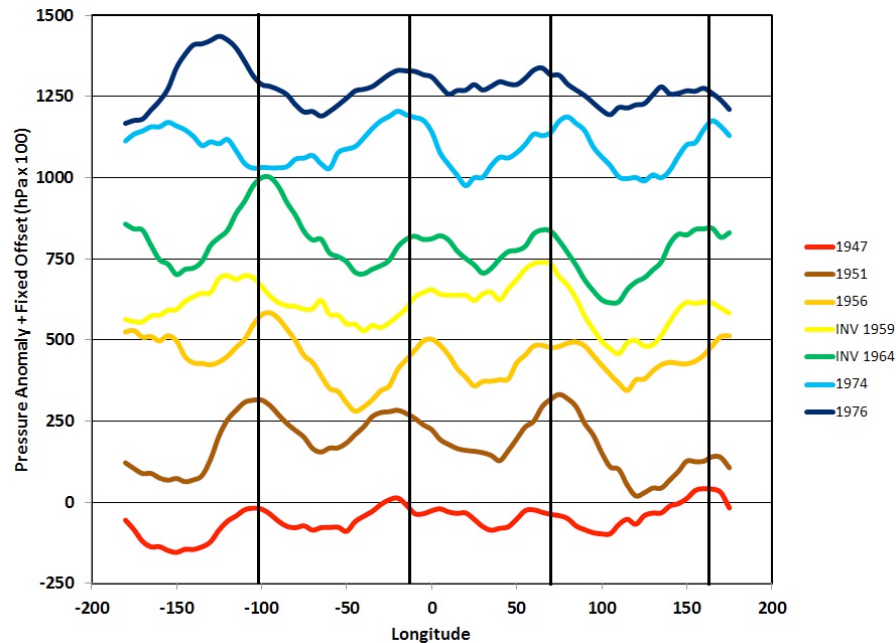


**Fig. (2a).** A plot of the average MSLP anomaly between the latitudes of 20° S and 50° S, as a function of longitude. The longitudinal profiles are shown for those years between 1947 and 1976 that exhibit an N=4 standing wave-like zonal pattern similar to the one that appeared in the Southern Summer of 1981. Arbitrary fixed offsets have been applied to the MSLP anomalies to vertically separate the longitudinal profiles.
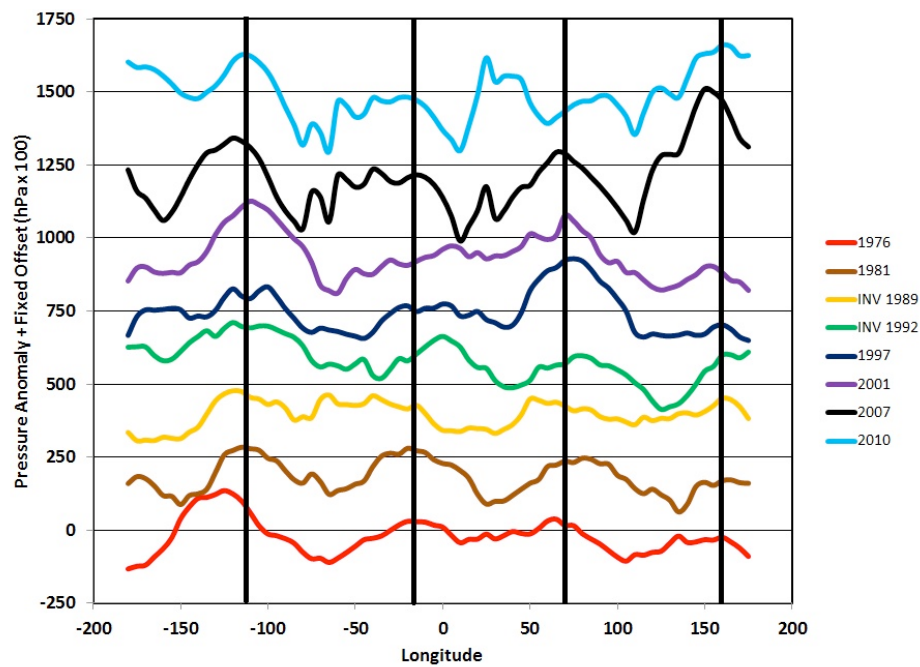
**Fig. (2b).** The corresponding plot for the years between 1976 and 2010.
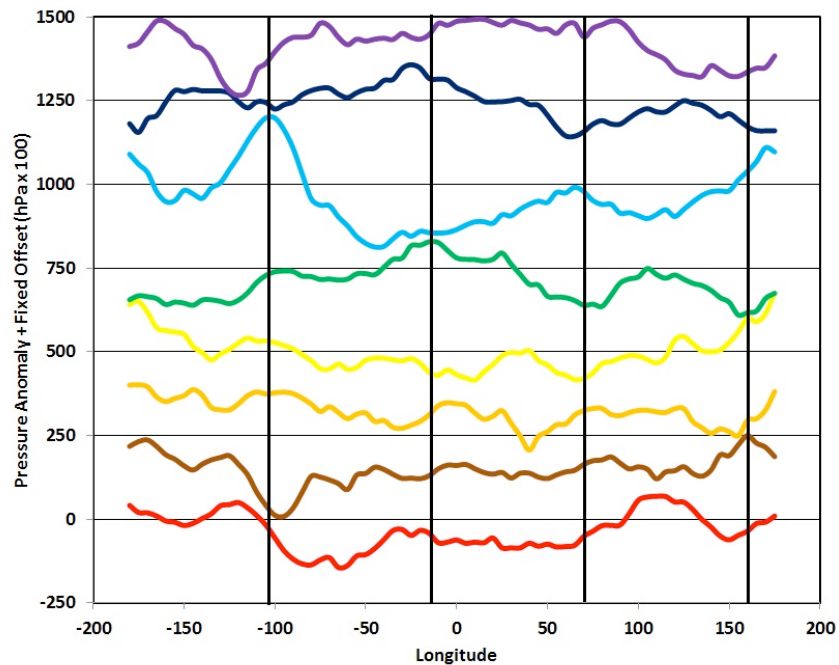


**Fig.(2c).** A plot of the average MSLP anomaly between the latitudes of 20° S and 50° S, as a function of longitude, for those years between 1947 and 1979/80 that are three years after the years shown in sequence B.

the latitudes of 20° S and 50° S, as a function of longitude. The longitudinal profiles are shown for those years between 1947 and 1976 that exhibit an N=4 standing wave-like zonal pattern similar to the one that appeared in the Southern Summer of 1981. Arbitrary fixed offsets have been applied to the MSLP anomalies to vertically separate the longitudinal profiles. Fig. (**2b**) shows the corresponding plot for the years between 1976 and 2010.

Columns one and three of Table **1** show the longitudinal MSLP anomaly profiles displayed in Fig. (**2a, b**), arranged in order of increasing time. These columns demonstrate that there is a sequence (A) of southern summers, starting in

1947 and ending in 2007, with an average separation of 8.6 years, that have an N=4 standing wave-like zonal pattern in the MSLP anomalies similar to that seen in the summer of 1981 [N.B. that for four of the years: 1959; 1964; 1989; and 1992, the longitudinal profiles have been inverted to match the other profiles]. They also show that there is a parallel sequence (B) that starts three years later in 1951 and ends three years later in 2010, that closely matches the spacing of the first sequence, with an average separation of 8.4 years.

In contrast, Fig. (**2c**) shows the average MSLP anomaly between the latitudes of 20° S and 50° S, as a function of longitude, for those years between 1947 and 1979/80 that are
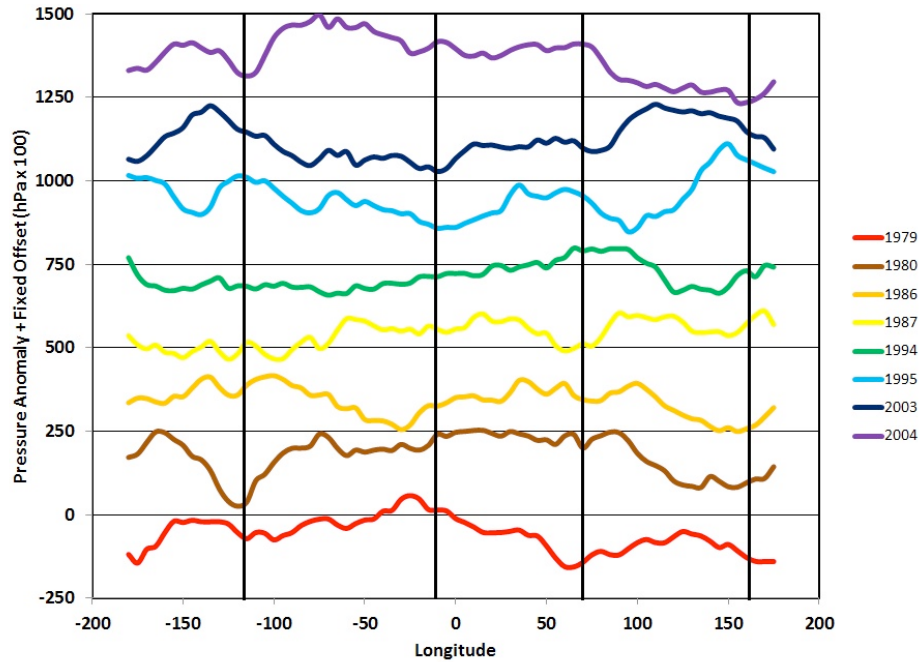
**Fig. (2d).** The corresponding plot for the years between 1979/80 and 2010.

**Table 1.    Columns One and Three: The Longitudinal MSLP Anomaly Profiles Displayed in Fig. (2a, b), Arranged in Order of Increasing Time. Columns Two and Four: The Spacing Between the Consecutive Events in Columns One and Three, Respectively. Column Five: The Longitudinal MSLP Anomaly Profiles that are Displayed in Fig. (2c, d), Arranged in Order of Increasing Time. These Years are Specifically Chosen to Avoid Those Years Found in Either Column One or Three. Column Six: The Spacing (in Years) Between the Consecutive Events in Column Five**

| A | Δ Years | B | Δ Years | C | Δ Years |
|---|---|---|---|---|---|
| 1947 | – | 1951 | – | 1954/55 | – |
| 1956 | 9 | **1959** | 8 | 1962/63 | 8 |
| **1964** | 8 | 1967 | 8 | 1970/71 | 8 |
| 1974 | 10 | 1976 | 9 | 1979/80 | 9 |
| 1981 | 7 | 1984 | 8 | 1986/87 | 7 |
| **1989** | 8 | **1992** | 8 | 1994/95 | 8 |
| 1997 | 8 | 2001 | 9 | 2003/04 | 9 |
| 2007 | 10 | 2010 | 9 | – | – |
| Average Spacing | **8.6** Years | Average Spacing | **8.4** Years | Average Spacing | **8.2** Years |

three years after the years shown in sequence B. Fig. (**2d**) shows the corresponding plot for the years between 1979/80 and 2010 [N.B. one additional year either side of the particular year in question is displayed to demonstrate that we have not selectively chosen years that support our claim].

Column five of Table **1** shows the longitudinal MSLP anomaly profiles displayed in Fig. (**2c, d**), arranged in order of increasing time. The years in column five of Table **1** are specifically chosen to be representative of times that avoid those found in either sequence A or sequence B.

Inspection of Fig. (**2c, d**) show that the longitudinal profiles for the particular years listed in column 5 rarely display the classic N=4 standing wave-like pattern that is evident in the years that are listed in sequences A and B.

Hence, Fig. (**2a-d**) and Table **1** indicate that the MSLPs of the four semi-permanent high pressure systems are being simultaneously enhanced by a N=4 standing wave-like zonal pattern in MSLP anomalies that is propagating around the Southern Ocean with a period that closely matches the period of the 18.6/9.3 year draconic spring tides. This alone justifies our further investigation of the potential long-term effects of the draconic lunar atmospheric tides upon the general atmospheric circulation patterns of the Southern Hemisphere.

In section 2, the MSLP anomaly data and the merged land and SST anomaly data used in this study are presented. This is followed by a brief discussion of the latitude restrictions that are placed upon the anomaly maps by the data quality. These latitude limits are used to determine what data can be productively used to search for long-term changes in the MSLP and SST anomaly maps of the Southern Hemisphere.

The initial plan was to use the summer (DJF) MSLP and SST anomaly maps covering a 60 year period from 1940 to 2000, dividing the data up into two 30 year climate epochs, with the year 1970 as the common boundary point. However, due to the poor quality of the MSLP and SST anomaly data prior to 1947, the anomaly maps chosen for the study were restricted to two adjacent climate epochs, each of which is 24 years in length. The first climate epoch is the 24 year period immediately prior to 1970 (i.e. 1947 to 1970) while the second is the 24 year period immediately following 1970 (i.e. 1971 to 1994).

[N.B. The year 1970 was chosen because it represented a pivotal point in the evolution of the global structure of the Earth's atmosphere during the latter part of 20th Century. For the thirty year period prior to 1970 (i.e. 1940 to 1970), the Earth's atmosphere was characterized by a meridional circulation pattern (as measured by the Vangengeim-Girs or Atmospheric Circulation Index - ACI) and decreasing mean world temperatures. This was followed by a thirty year period after 1970 (i.e. 1970 and 2000), where the Earth's atmosphere was characterized by a zonal circulation pattern (as measured by the ACI) and increasing mean world temperatures (Gris [13], Sidorenkov and Svirenko [14], Sidorenkov [15]).

In section 3, the longitudinal shift-and-add method is used to search for periodic spatial features in the Summer (DJF) MSLP and SST anomaly data, that are moving zonally (east-west) around the Earth at constant longitudinal drift rates.

Finally, the main results of this investigation are presented in Section 4 and the discussion and conclusions are outlined in section 5.

## 2. DATA

### 2.1. The Mean Monthly Sea Level Atmospheric Pressure Data

The UK Met Office Hadley-Centre (UKMO) has published a data set called hadSLP2.asc (Adam and Ansell [11]) that contains the MSLP, averaged over 5 x 5 degree latitude-longitude bins, for the Southern Hemisphere between the years (January) 1850 and 2004 (U.K. Metoffice [16]). This paper uses a modified version of the UKMO hadSLP2.asc data set called hadSLP2r.asc. The hadSLP2r. asc file has been created by extending the hadSLP2.asc data from 2004 up to October 2010, using monthly NCEP/NCAR data (U.K. Metoffice [16]).

The interpolated data in the hadSLP2r.asc file has "valid" data values in all of its gridded cells. However, if a comparison is made between the interpolated data set hadSLP2r.asc and the un-interpolated data set hadSLP2.0_act.asc (U.K. Metoffice [16]), it is immediately obvious that there are very few raw data values in the gridded cells south of 45° – 50° S latitude.

Indeed, for gridded cells sharing the same latitude, only those with latitudes ≤ 40° S have ≤ 1/3 of their data values missing throughout most of the first climate epoch (i.e. from 1947 to 1970). Similarly, for gridded cells sharing the same latitude, only those with latitudes ≤ 45° S have ≤ 1/3 of their data values missing throughout most of the second climate epoch (i.e. from 1971 to 1994).

This means that most of the gridded values in the interpolated data set hadSLP2r.asc with latitudes south of 40° S, during the first climate epoch, and south of 45° S, during the second climate epoch, have so few measured data values that they must have been estimated by a process of extrapolation, rather than interpolation.

This is confirmed in Fig. (**3a**, **b**) using MLSP measurements from the un-interpolated data set hadSLP2.0_act.asc. Fig. (**3a**) shows a map of MSLP for the whole of the Southern Hemisphere for January 1950 and Fig. (**2b**) shows the corresponding plot for January 1971 (N.B. these particular pressure maps have been chosen because they are typical of the two climate epochs in question). Dark black horizontal lines have been drawn across Fig. (**3a**) at a latitude of 45° S and Fig. (**3b**) at a latitude of 50° S. These lines have been superimposed on these figures to highlight the most southerly latitude at which most of the gridded values in the interpolated data set were derived by either a process of interpolation or by limited extrapolation from adjacent gridded cells.

Fig. (**3a**, **b**) show that if you want to minimize potential errors in the gridded MSLP data values that are caused by uncertainties associated with extrapolation, you need to treat with suspicion all of the data values in the final adopted data set that are south of 45° latitude for the first climate epoch and south of 50° latitude for the second climate epoch.

Finally, the MSLP value for each gridded data point has been converted to a pressure anomaly by subtracting the MSLP, averaged over the climate epoch for that data point i.e. the MSLP for gridded data points in the first climate epoch were normalized to the mean for the years 1947 to 1970 and the MSLP for gridded data points in the second climate epoch were normalized to the mean for the years 1971 to 2000. The reason for this period-specific normalization will be explained in section 3.

### 2.2. The Merged Sea Surface and Land Surface Temperature Anomaly Data

This study uses the NOAA National Climate Data Centre merged land and ocean surface temperature anomalies (NOAA_NCDC [17] – File: ncdc_blended_merg53v3b.dat. gz as accessed on 10th Dec 2009) to map global temperature variability and trends in the Southern Hemisphere between the years 1940 and 2000.

The temperature anomaly data set is formed from the merging of the Global Historical Climatology Network-Monthly (GHCN-M) version 2 station land surface temperature anomalies with the ERSST version 3b gridded SST anomalies. The gridded anomalies for the GHCN-M.v2 and ERSST.v3 data sets are obtained by averaging the anomalies within 5° × 5° gridded boxes covering the whole of the Southern Hemisphere.

Unlike the UKMO atmospheric pressure data in section 2.1, the NOAA merged land and ocean surface temperature anomaly data does not use a process of interpolation/ extrapolation to fill in all the gridded cells with "valid" data. Instead, the NOAA surface temperature anomaly data set assigns a value of -9999 to each of the gridded cells that contain no data. This means that we must fill in the missing data by a process of interpolation.
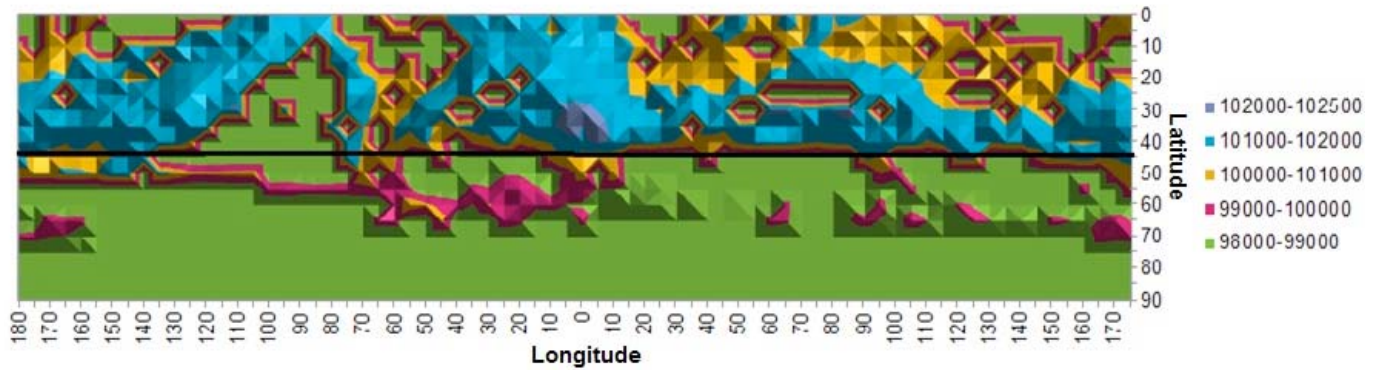
**Fig. (3a).** A map of MSLP for the whole of the Southern Hemisphere for January 1950. A dark black horizontal line has been drawn across this figure at a latitude of 45° S. This line is designed to highlight the most southerly latitude at which most of the gridded values in the interpolated data set were derived by either a process of interpolation or by limited extrapolation from adjacent gridded cells.
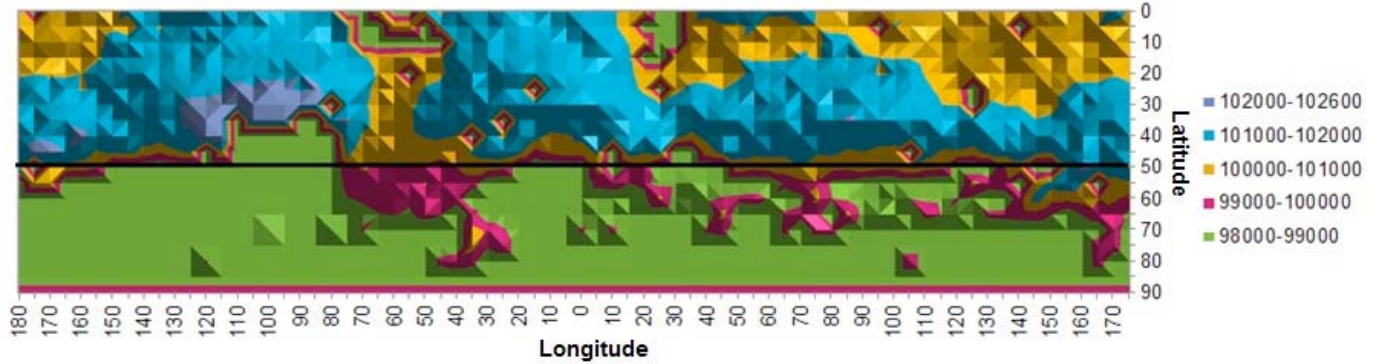


**Fig. (3b).** A map of MSLP for the whole of the Southern Hemisphere for January 1971. A dark black horizontal line has been drawn across this figure at a latitude of 50° S. This line is designed to highlight the most southerly latitude at which most of the gridded values in the interpolated data set were derived by either a process of interpolation or by limited extrapolation from adjacent gridded cells.

For the purposes of interpolation, the gridded NOAA merged land and ocean surface temperature anomaly data was broken up into a set of individual longitudinal profiles. Each of these profiles was formed by grouping together all of the cells that shared the same latitude and then arranging them in order of increasing longitude from 180° W to 175° E. Missing data cells in each of these longitudinal profiles were filled in by using a simple process of linear interpolation with longitude. Given the crudeness of interpolation method used, only those longitudinal profiles with a maximum of ten contiguous missing data cells, and 12 missing data cells in total, per longitudinal profile of 72 gridded cells, were considered to have sufficient quality to reliably track temporal and spatial changes in the distribution of SST anomalies.

The screening criteria that are used for contiguous missing data cells are met by all those longitudinal profiles between the years 1947 and 1970 that have latitudes ≤ 40° – 45° S, with the exception of January 1948 [11 contiguous missing data cells and 16 missing data cells in total]. However, the longitudinal profiles for this particular month were incorporated with all of the other longitudinal profiles to provide a continuous data set from 1947 to 1970, since the effects of their inclusion upon the quality of the final data set should be minimal.

Similarly, the screening criteria that are used for contiguous missing data cells are met by all those

longitudinal profiles between the years 1971 and 2000 that have latitudes ≤ 45° – 50° S.

Fig. (**4a**) shows a map of the un-interpolated NOAA National Climate Data Centre's merged ocean and land surface temperature anomalies for the whole of the Southern Hemisphere for January 1947. Fig. (**4b**) shows the corresponding plot for February 1978. The units of colour gradation are in 1/100th of a degree Celsius [N.B. these particular anomaly maps have been chosen because they highlight the regions were interpolation is used to fill in missing data for the two climate epochs in question]. Dark black horizontal lines have been drawn across Fig. (**4a**) at a latitude of 45 – 50 ° S and Fig. (**4b**) at a latitude of 50 – 55° S, marking latitudes that are five degrees south of the respective southern limits of the high quality data.

The dark line in Fig. (**4a**) at 45 – 50° S highlights the fact that most of the missing data between the years 1947 and 1970 is located just off the Pacific Coast of South America, centred near longitude 100° W. It also shows that longitudinal temperature anomaly profiles start to become heavily affected by missing data south of 50° S.

In like manner, the dark line in Fig. (**4b**) at 50 – 55° S shows that most of the missing data between the years 1971 and 2000 is also located just off the Pacific Coast of South America, this time centred near longitude 115° W. It also shows that longitudinal temperature anomaly profiles start to become heavily affected by missing data south of 55° S.
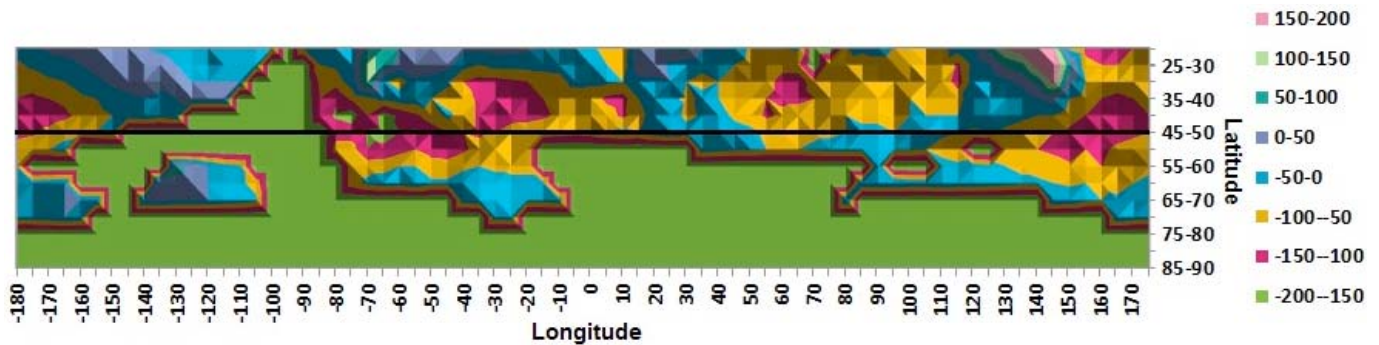
**Fig. (4a).** A map of the un-interpolated NOAA National Climate Data Centre's merged ocean and land surface temperature anomalies for the whole of the Southern Hemisphere for January 1947. A dark black horizontal line has been drawn across this figure at a latitude of 45 – 50 ° S. The units used for SST in this paper are 1/100th of a degree Celsius, unless noted otherwise.
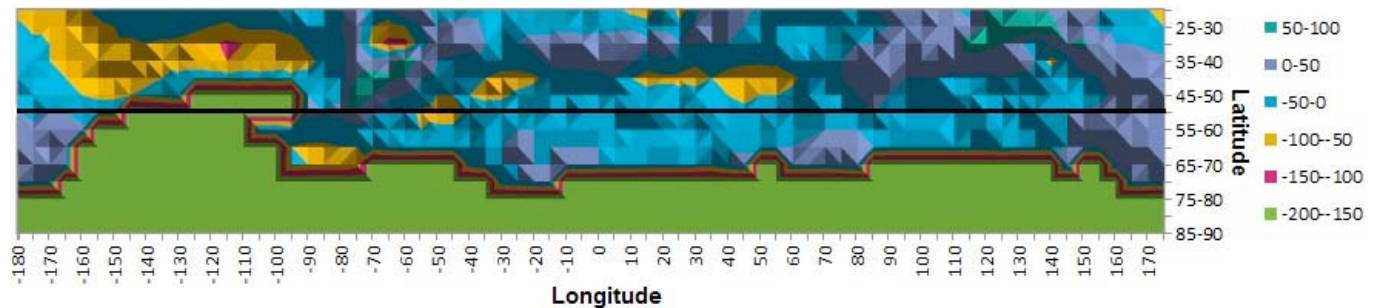


**Fig. (4b).** A map of the un-interpolated NOAA National Climate Data Centre's merged ocean and land surface temperature anomalies for the whole of the Southern Hemisphere for February 1978. A dark black horizontal line has been drawn across this figure at a latitude of 50 – 55° S.

## 3. METHODS

The longitudinal shift-and-add method used in this paper is designed to search for periodic spatial features in the mean Summer (DJF) MSLP and SST anomaly maps that are moving zonally (east-west) around the Earth at a constant longitudinal drift rate per year.

The first step of the longitudinal shift-and-add method is to choose a base year. The logical choice is the first year of the given climate epoch that is under consideration i.e. 1947 for the first climate epoch (1947 to 1970) and 1971 for the second climate epoch (1971 to 1994).

The second step is to add the mean summer anomaly map for each subsequent year in the climate epoch, to the mean summer anomaly map of the base year, after a correction is made for a constant rate of longitudinal shift of that particular anomaly map from the base year.

The third step is to repeat step two for a number of different fixed longitudinal shift rates and then see if there are any patterns that persist in the final stacked anomaly maps.

The beauty of the longitudinal shift-and-add method is that most SST or MSLP anomaly patterns that are not drifting at the selected longitudinal drift rate will be quickly smeared out and lost in the noise. Of course, this includes any MSLP and SST anomalies patterns that are fixed in longitude as well.

Finally, the stacked anomalies maps are used to produce a series of longitudinal profiles of the summer (DJF) MSLP

and SST anomalies for a series of different longitudinal drift rates.

The power spectral densities for each longitudinal profile are then calculated in order to determine the relative spectral power that is associated with any N=4 standing wave-like features that might be present in the summer MSLP and SST anomaly profiles. These power spectral density values are plotted against the westerly drift rate.

There are two immediate problems associated with the longitudinal shift-and-add method.

These are that:

1.   spatial features like those we are searching for that have a longitudinal period of 90° and are moving with a constant westerly longitudinal drift rate (DR in degrees per year) can produce exactly the same results as spatial features with the same longitudinal period that are moving with a constant easterly longitudinal drift rate of (90° – DR). This means that care must be taken to resolve the ambiguity in the direction of movement of any spatial features that are detected [see Appendix **A** for a resolution of this ambiguity].

2.   the MSLP and SST anomalies in each of 5° x 5° cells of the anomaly maps for a given 24 year climate epoch needs to be normalized to the respective averages for that particular climate epoch. This is necessary because using the average values for another climate epoch introduces spatial structure into the final summed anomaly maps that is representative of the slow regional drift in MSLP anomalies and SST anomalies between the two climate epochs.

Finally, there are additional problems with the longitudinal shift-and-add method. However, an explanation of these problems will be delayed until Section 4, since they are best explained with reference to the summed anomaly maps and their corresponding longitudinal profiles.

## 4. RESULTS

### 4.1. Climate Epoch: 1971 to 1994

#### *4.1.1. The Southern Summer (DJF) Mean Sea-Level Pressure Anomalies*

Fig. (**5**) shows the relative power spectral density (PSD) for features that have an N=4 pattern in the longitudinal profiles (averaged between latitudes 30° and 50° S) that are extracted from the shift-and-add maps of the summer MSLP anomalies. The PSDs are plotted against their westerly longitudinal drift rates which range from 0 to 90° per year, in steps of 5° per year [N.B. The maximum drift-rate in Fig. (**5**) is limited to 90° because of the ambiguity that results from rotating an N=4 longitudinal pattern by ≥ 90°]. A dark horizontal line is drawn across the bottom of Fig. (**5**)

showing the 99 % confidence limit (see the diagrams figure caption for details).

As was noted in section 3, care must be taken in interpreting the results shown in Fig. (**5**). One problem with the method is that it is possible to produce an illusionary drift in a stationary [i.e. non-drifting] N=4 pattern simply by modulating the amplitude of the structures seen in the MSLP and SST anomalies longitudinal profiles on time scales that are whole multiples of the annual sampling rate. For example, given that a longitudinal N=4 pattern consists of four fixed structures that are separated in longitude by 90°, simply sampling this pattern on an annual basis, will produce a peak in the relative PSD at a drift rate of 90° per year even though the pattern itself is not moving. Similarly, peaks in the PSD would be produced by biennial modulations of the structure's amplitudes seen in the MSLP and SST anomalies at drift rates of 45° and 90° per year, by triennial modulations at drift rates of 30°, 60° and 90° per year, and so on. Clearly, if the longitudinal profiles for the shift-and-add maps for the summer MSLP and SST anomalies have a
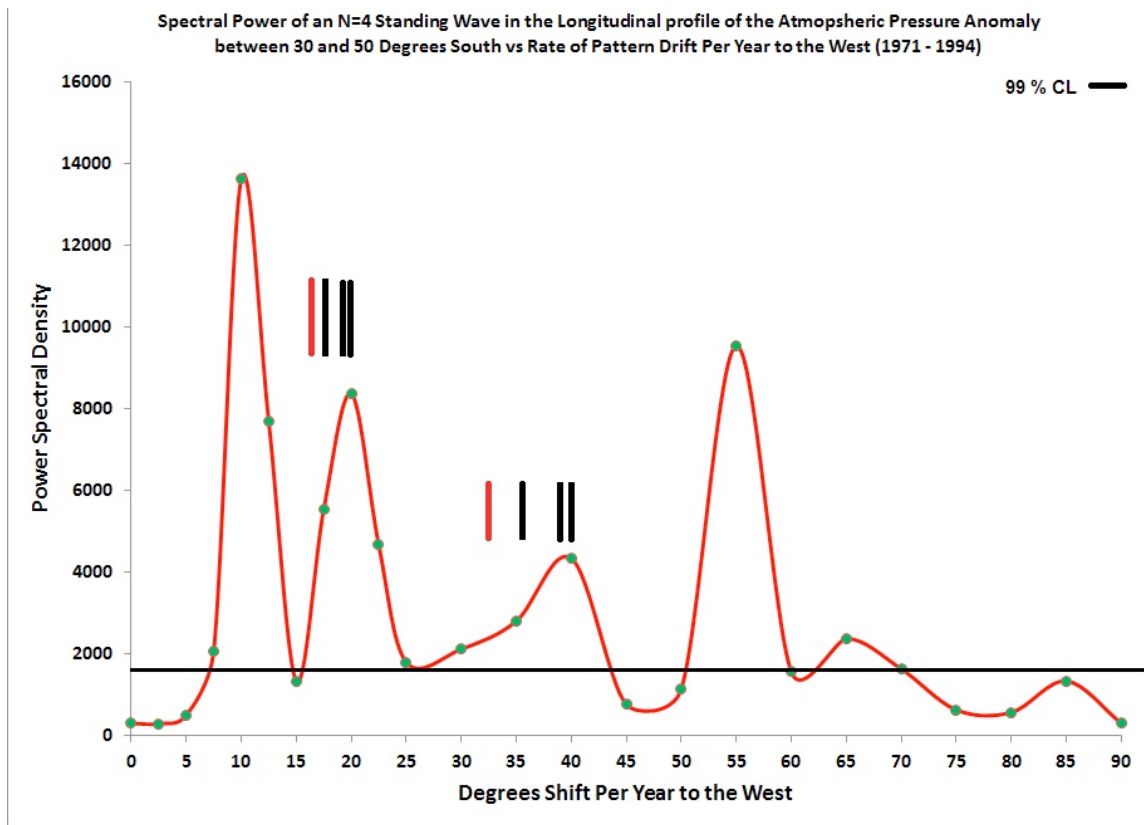


**Fig. (5).** The relative power spectral density (PSD) for those features that have an N=4 pattern in the average longitudinal profile for latitudes between 30° and 50° S, for the shift-and-add map of the summer MSLP anomalies, plotted against westerly longitudinal drift rate. N.B. The step in westerly drift rates has been increased to 2.5° per year between 0 and 25° degrees per year for greater resolution. A solid black line drawn across the lower part of this figure indicates the minimum power spectral density that is required to rule out the possibility that the signal is generated by noise at the 0.01 (= 99 %) confidence limit. This limit was obtained by applying the Multi-Taper Method (MTM) (number of tapers =3) to each shift-and-add anomaly profile that is associated with a given drift rate in this diagram. Only those points which had spectral densities that could not be generated by chance from either white noise or AR(1) noise at the 0.01 level were accepted as being statistically significant. All points above the 99 % confidence line in this figure are statistically significant while all the points below this line are not (with the exception of the point with a drift-rate of 50° per year). It is important to note that there are strong, low frequency spatial features present in the individual spatial MSLP anomaly profiles. Under these circumstances, simple spectrogram analysis is not good at determining the true spectra noise levels that are need to test the statistical significance of spectral features. One way to circumvent this problem is to use MTM analysis, since it better able to distinguish strong low frequency signals from spectral noise.

non-zero PSD for drift rates of 0° per year then care must be taken to ensure that the peaks in the PSD at non-zero drift rates are not falsely indicting pattern drift.

If the analysis of Fig. (**5**) is limited to westerly drift rates that are less than 45°, then there are three drift rates that show prominent N=4 patterns in their summer MSLP anomaly profiles. The first is at a fixed westerly drift rate of 10° per year in longitude (time to circumnavigate the Earth ≈ 36 years), the second is 20° per year (circumnavigation time ≈ 18 years) and the third is 40° per year (circumnavigation time ≈ 9 years).

The interpretation given to the first three peaks in Fig. (**5**) are confirmed in Fig. (**6a-c**). These figures show shift-and-add maps of the Southern Hemisphere MSLP anomalies between the latitudes of 20° and 60° S for westerly longitudinal drift rates of 0°, 10°, and 20° per year, respectively [N.B. Pressure anomalies are plotted so that lower-than-normal MSLP anomalies are displayed as positive numbers].

Fig. (**6a**) shows no obvious features with longitudinal periodicity (Hence, the peaks in PSD seen in Fig. (**5**) cannot be produced by multi-annual modulation of a stationary N=4 pattern in the MSLP anomaly profiles). This is in agreement with the low PSD at a zero drift rate that is evident in Fig. (**5**). In contrast, both Fig. (**6b, c**), (with westward drift rates of 10° and 20° per year), show distinct longitudinal patterns that resemble an N=4 standing wave straddling the Earth at a mean latitude of 45° S. Again, this is in agreement with the peaks in PSD that are seen near 10° and 20° per year in Fig. (**5**).

In order to more precisely identify the actual circumnavigation time that is associated with the peak in PSD at 20° per year shown in Fig. (**5**), a set of four vertical lines has been placed above this peak. From left to right, these lines correspond to circumnavigation times that are equal to the solar Hale cycle (22 years), the lunar Perigee-Syzygy cycle (20.3 years), the lunar Draconic cycle (18.6 years) and the lunar Saros (or Eclipse) cycle (18.0 years). A similar set of four verticals lines also appears above the sub-harmonic peak with a drift rate of 40° per year. These four lines correspond to circumnavigation times at 11.0, 10.15, 9.3, and 9.0 years. It is evident from this comparison that the circumnavigation times that best match to the positions of these two peaks are those of the 18.6 year lunar Draconic or the 18.0 year lunar Saros cycles.

Hence, Figs. (**5, 6a-c**) indicate that there are four extended features of lower-than-normal pressure in the summer MSLP anomalies which are centred between 30 and 50° S and separated from each other by approximately 90° in longitude (i.e. there is an N=4 pattern in the longitude profile). In addition, these figures show that, over the 1971 to 1994 climate epoch, these patterns are drifting in longitude at rates that produce circumnavigation times that match either the length of the 18.6 year lunar Draconic cycle or the 18.0 year lunar Saros cycle.

Fig. (**5**) also shows that there are three additional peaks in the power spectral density with longitudinal drift-rates of 55°, 65° and 85° per year westward. These three peaks appear to repeat the relative spacing of the three peaks at 10°, 20°, and 40°, except for the fact that they're longitudinal drift-rates are systematically larger by 45° per year i.e. 55° (= 10° + 45°), 65° (= 20° + 45°), and 85° (= 40° + 45°). The simplest explanation for the drift rates at 55°, 65°, and 85° is that there is a quasi-biennial variation in the strength of the drifting N=4 pattern that is present in the summer MSLP
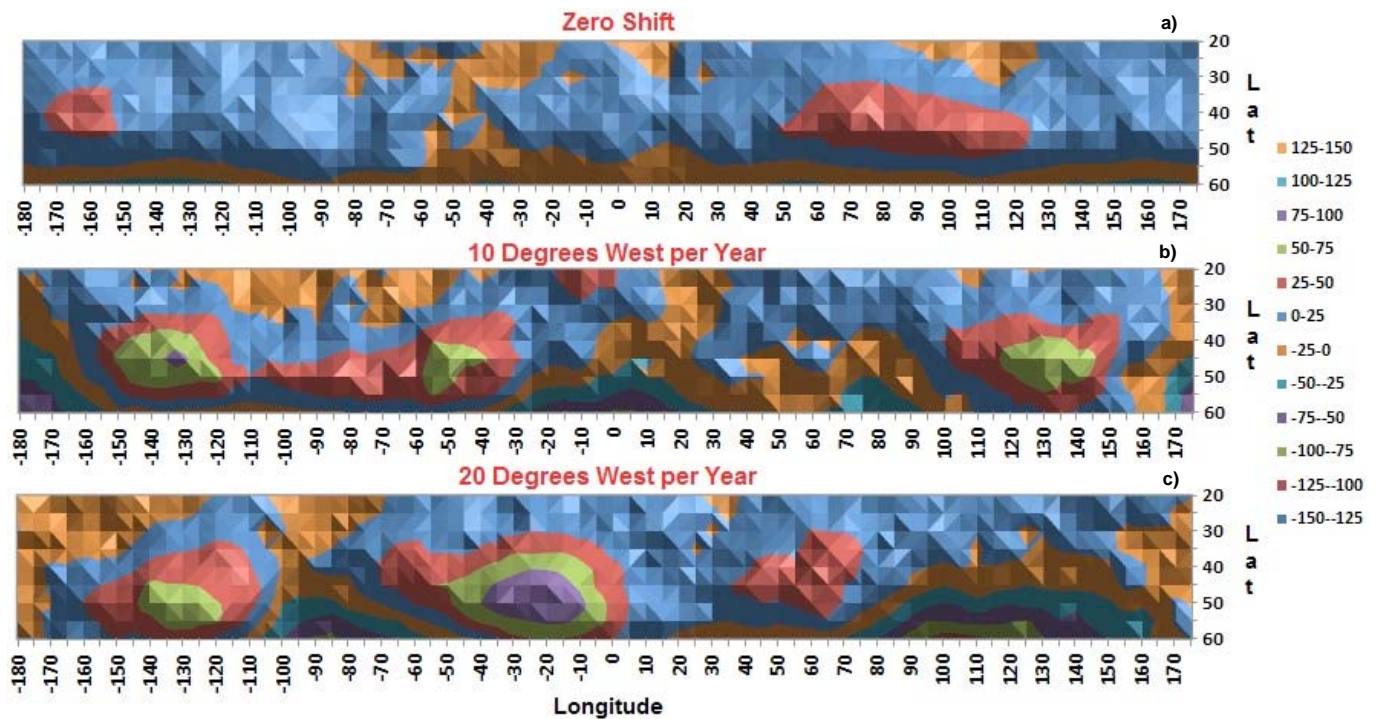


**Fig. (6).** (**a-c**) The shift-and-add maps of the Southern Hemisphere MSLP anomalies between the latitudes of 20° and 60° S for westerly longitudinal drift rates of 0°, 10°, and 20° per year, respectively. The pressure anomalies are plotted so that lower-than-normal MSLP anomalies are displayed as positive numbers.

anomaly profiles. Since the prominent structures in the N=4 pattern are separated in longitude by roughly 90°, it is possible for these structures to mimic a westerly movement of 55°, 65°, and 85° per year by moving at 10°, 20°, 40° per year to the west, respectively, provided that the standing wave-like structures are preferentially enhanced once every second year. Of course, the reverse is also true i.e. a pattern moving towards the west at 10°, 20°, 40° per year could also be mimicked by a pattern moving at 55°, 65°, and 85° per year to the west, respectively, provided that the standing wave-like structures are preferentially enhanced once every second year.

Fig. (**7a**) shows the shift-and-add map for a drift rate of 10° per year for all the years between 1971 and 1994. Fig. (**7b**) shows the corresponding plot for the shift-and-add map that includes only the even years, over the same climate epoch. Finally, Fig. (**7c**) shows the corresponding shift-and-add map that includes only the odd years between 1971 and 1994.

A comparison of Fig. (**7b, c**) with Fig. (**7a**) clearly shows that the N=4 pattern is much more prominent in the odd years than it is in the even years. Hence, the presence of a strong biennial modulation of the structures in the shift-and-add anomaly maps, combined with the two almost equally strong peaks in PSD at 10° and 55° per year seen in Fig. (**5**), introduces an ambiguity in the drift rate for these values, since each drift rate is capable of mimicking the other, provided the structures are preferentially enhanced every second year.

Finally, the relatively weakness of the two peaks in PSD at 65° and 85° per year compared to those at 20° and 40° per year, indicates that the patterns are moving at the latter drift rates and they are only having their structures modified by weak biennial modulations.

### 4.1.2. The Southern Summer (DJF) Mean Sea-Surface Temperature Anomalies

Fig. (**8**) shows the relative PSD for features that have an N=4 pattern in the average longitudinal profile between 20° and 40° S, for the shift-and-add map of the summer mean SST anomaly, plotted against westerly longitudinal drift rate. The westerly drift rates in Fig. (**8**) range from 0 to 90° of longitude per year, in steps of 5° per year. A dark horizontal line is drawn across the bottom of Fig. (**8**) showing the 99 % confidence limit (see the diagrams figure caption for details).

Fig. (**8**) shows that there are two drift rates that have prominent N=4 patterns in their summer SST anomaly profiles. The first is at a fixed westerly shift rate near 17.5° per year in longitude (time to circumnavigate the Earth ≈ 20.6 years), the second is near 35° per year (circumnavigation time ≈ 10.3 years).

This interpretation in confirmed by Fig. (**9a-c**) which show the shift-and-add maps of the Southern Hemisphere SST anomalies between the latitudes of 20-25° and 55-60° for three different drift rates. Fig. (**9a**) shows the map for no drift between 1971 and 1994, Fig. (**9b**) the map for a drift of 17.5° per year to the west, and Fig. (**9c**) the map for a drift of 35° per year to the west.

There are no obvious features that have ordered longitudinal periodicity evident in Fig. (**9a**).

This is in agreement with the low PSD at a zero drift rate that is evident in Fig. (**8**, i.e. the peaks in PSD seen in this figure cannot be the result of multi-annual modulations of a stationary N=4 pattern in the MSLP anomaly profiles). In contrast, both Fig. (**9b, c**, with respective westward drift rates of 17.5° and 35° per year), show features that exhibit a longitudinal periodicity that resemble that of an N=4 pattern
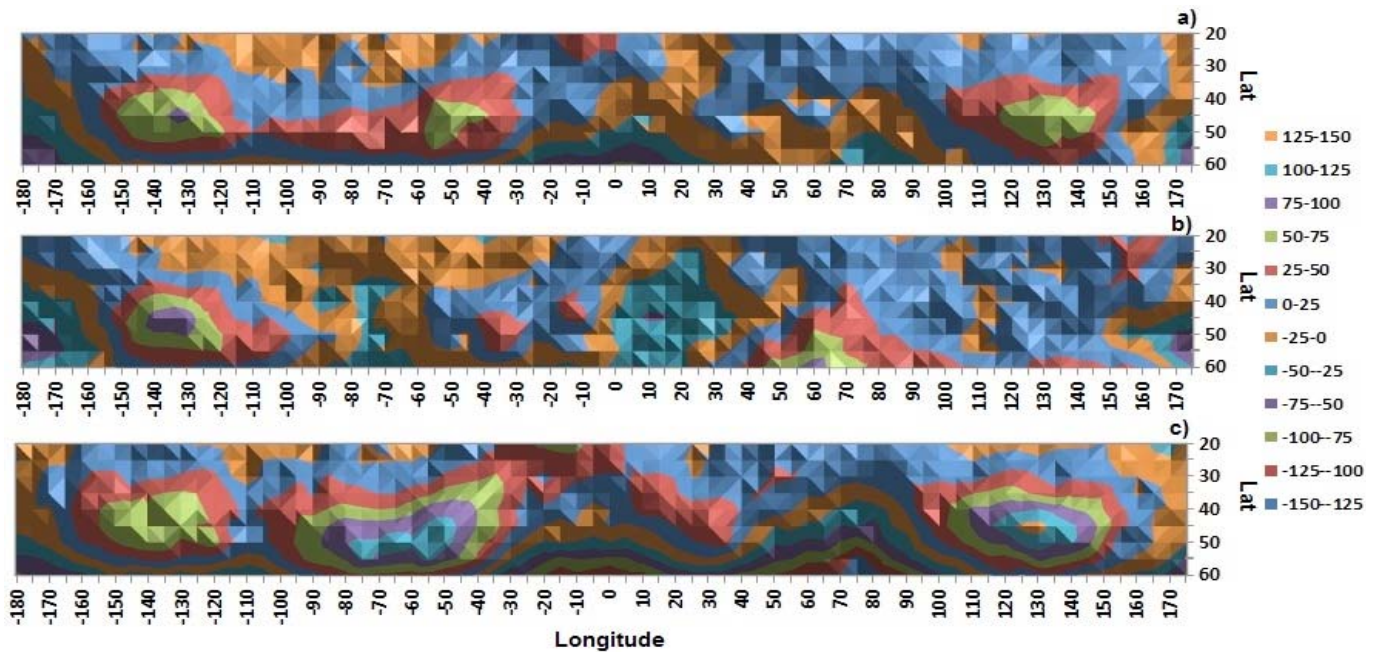


**Fig. (7).** (**a**) The shift-and-add map for a drift rate of 10° per year for all the years between 1971 and 1994. (**b**) The corresponding shift-and-add map that includes only the even years, over the same climate epoch. (**c**) The corresponding shift-and-add map that includes only the odd years.
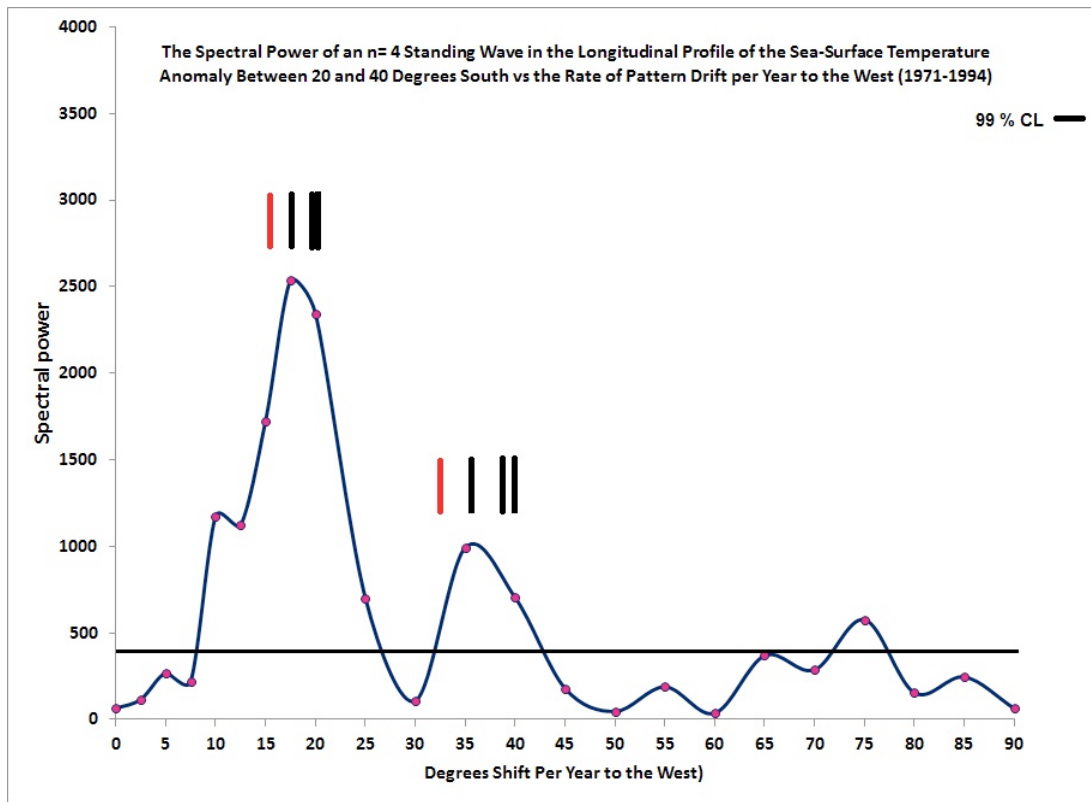
**Fig. (8).** The relative PSD for features that have an N=4 pattern in the average longitudinal profile between 20° and 40° S, for the shift-and-add map of the summer mean SST anomaly, plotted against westerly longitudinal drift rate. A solid black line drawn across the lower part of this figure indicates the minimum power spectral density that is required to rule out the possibility that the signal is generated by noise at the 0.01 (= 99 %) confidence limit. This limit was obtained by taking a Lomb-Scargle Periodogram (LSP) of each shift-and-add anomaly profile that is associated with a given drift rate in this diagram. Since the data is evenly spaced in time, taking the LSP is equivalent to taking the PSD of the longitudinal profiles. The LSP method is used in preference to MTM analysis with this data because low-frequency spatial features present in the individual shift-and-add SST anomaly profiles are not as strong as those seen in the MSLP anomaly profiles (see the caption for Fig. **5**). The confidence limit line shown in this figure is actually the line-of best fit to a set of confidence limit points that have a power spectral density of $400 \pm 140$.
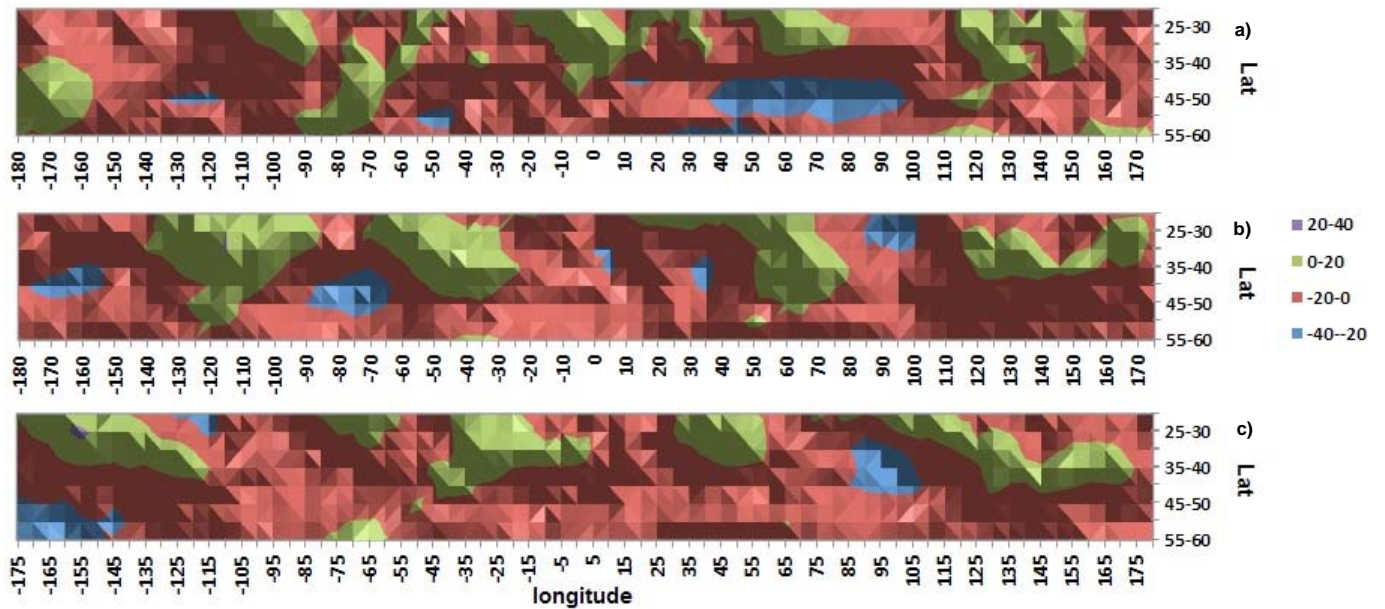


**Fig. (9).** (**a**) The shift-and-add maps of the Southern Hemisphere SST anomalies between the latitudes of 20-25° and 55-60° for (**9a**): no drift between 1971 and 1994. (**b**) A drift of 17.5° per year to the west. (**c**) A drift of 35° per year to the west. N.B. The step in westerly drift rates has been increased to 2.5° per year between 0 and 25° degrees for greater resolution.

straddling the Earth at a mean latitude of 30-35° S. Again, this is in agreement with the peaks in power spectral density that are seen at drift rates near 17.5° and 35° per year in Fig. (**8**).

As with Fig. (**5**), lines corresponding to circumnavigation times of the solar Hale cycle (22 years), the lunar Perigee-Syzygy cycle (20.3 years), the lunar Draconic cycle (18.6 years) and the lunar Saros (or Eclipse) cycle (18.0 years) have been placed above the peaks of PSD at 17.5° and 35° per year in order to more precisely identify the actual circumnavigation times associated with these peaks. It is evident from a comparison between the peaks and lines that the circumnavigation time that best matches the positions of the two peaks is the 20.3 year lunar Perigee-Syzygy cycle.

Thus, Figs. (**8**, **9a-c**) indicate that there are four extended features that have higher-than-normal summer SST which are centred between 25 and 45° S and that are separated from each other by approximately 90 degrees in longitude (i.e. there is an N=4 pattern in the longitude profile). In addition, these figures show that, over the 1971 to 1994 climate epoch, these patterns are drifting in longitude at rates that are most compatible with circumnavigation times that match the 20.3 year lunar Perigee-Syzygy cycle.

### 4.2. Climate Epoch: 1947 to 1970

#### 4.2.1 The Southern Summer (DJF) Mean Sea-Level Pressure Anomalies

Fig. (**10**) shows the relative power spectral density for those features that have an N=4 pattern in the average longitudinal profile for latitudes between 30° and 50° S, for the shift-and-add maps of the summer MSLP anomaly between 1947 and 1970, plotted against the westerly longitudinal drift rate.

Displayed in Fig. (**11a-d**) are the shift-and-add maps of the Southern Hemisphere MSLP anomalies for latitudes between 10 and 60 degrees, from 1947 to 1970, for westerly drift rates of 0°, 10°, 20°, and 40° per year, respectively [N.B. The pressure anomalies are plotted so that higher-than-normal MSLP anomalies are displayed as positive numbers].

Fig. (**10**) indicates that there is a non-zero PSD for a drift rate of 0° per year. Fig. (**11a**, i.e. the shift-and-add map for a drift rate of 0° per year) confirms that this PSD is associated with the four semi-permanent high pressure cells that are embedded in the Southern Hemisphere's sub-tropical high pressure ridge during the 1947 to 1970 climate epoch (Arhens [12]). Additionally, there are four other peaks in the PSD evident in Fig. (**10**) for drift rates less than 45° per year.
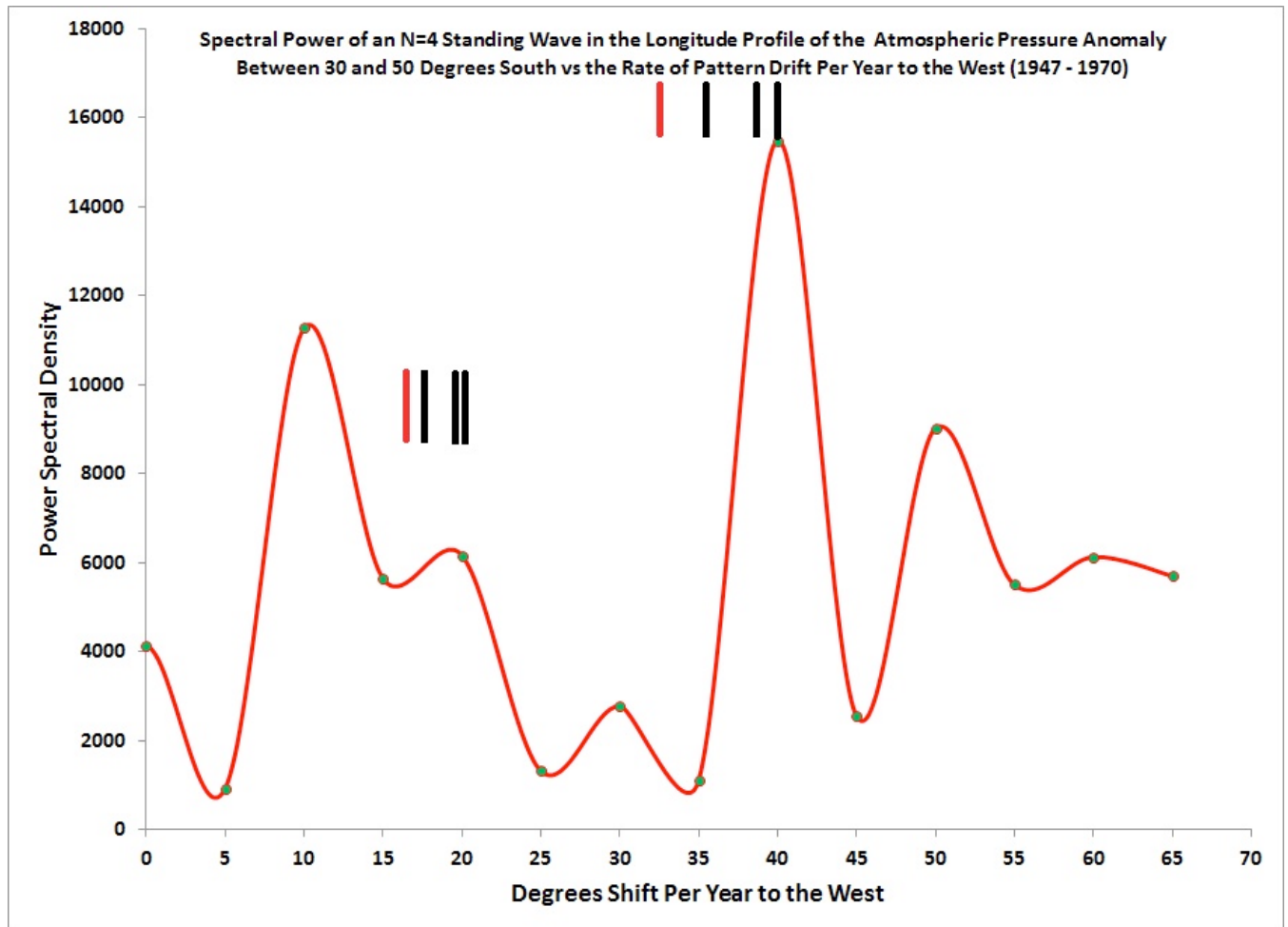


**Fig. (10).** The relative power spectral density for those features that have an N=4 pattern in the average longitudinal profile for latitudes between 30° and 50° S, for the shift-and-add maps of the summer MSLP anomaly between 1947 and 1970, plotted against the westerly longitudinal drift rate.

These peaks occur at drift rates of 10°, 20°, 30°, and 40° per year. A closer inspection of Fig. (**10**) reveals that the spacing of the peaks in PSD at drift rates of 0°, 10°, and 20° per year is repeated by the spacing of the peaks in PSD with respective drift rates of 30° (= 0° + 30°), 40° (= 10° + 30°), and 50° (= 20° + 30°).

The simplest possible explanation for the repetition in the spacing between the PSD peaks is similar to the reason given in section 4.1.1 i.e. it is possible to reproduce the peaks in the PSD at these higher drift rates (i.e. 30°, 40°, and 50° per year) if the N=4 patterns in the MSLP anomalies that are moving at 0°, 10°, and 20° per year are being preferentially enhanced once every third year. It is important to note, however, that it is also possible that there are N=4 patterns in the MSLP anomalies that are moving at the higher drift rates of 30°, 40°, and 50° per year, and it is these drifting patterns that are being triennially modulated to produce the peaks at drift rates of 0°, 10°, and 20° per year.

Fig. (**11c**, **d**, i.e. the shift-and-add maps with respective drift rates of 20° and 40° per year) both show remarkably similar longitudinal structures that resemble an N=4 pattern straddling the Earth at a mean latitude of ~ 45° S. It is these periodic patterns that produce the peaks in PSD that are observed near 20° and 40° per year in Fig. (**10**).

In comparison, Fig. (**11b**, i.e. the shift-and-add map with a drift rate of 10° per year) also shows an N=4 pattern is present at this drift rate. However, the pattern is displaced to the west by ~ 40° when compared to the patterns seen in Fig. (**11c**, **d**). The striking similarity of the longitudinal patterns seen in the shift-and-add maps for drift rates of 20° and 40° per year, contrasted with the pattern phase shift seen between the shift-and-add maps for drift rates 40° and 10° per year, supports the contention that most of the peak in PSD at 40° per year can be attributed to an N=4 pattern moving at 40° per year rather than a pattern moving at 10° per year that is being triennially modulated.

As with Fig. (**5**), lines corresponding to circumnavigation times of the solar Hale cycle (22 years), the lunar Perigee-Syzygy cycle (20.3 years), the lunar Draconic cycle (18.6 years) and the lunar Saros (or Eclipse) cycle (18.0 years)
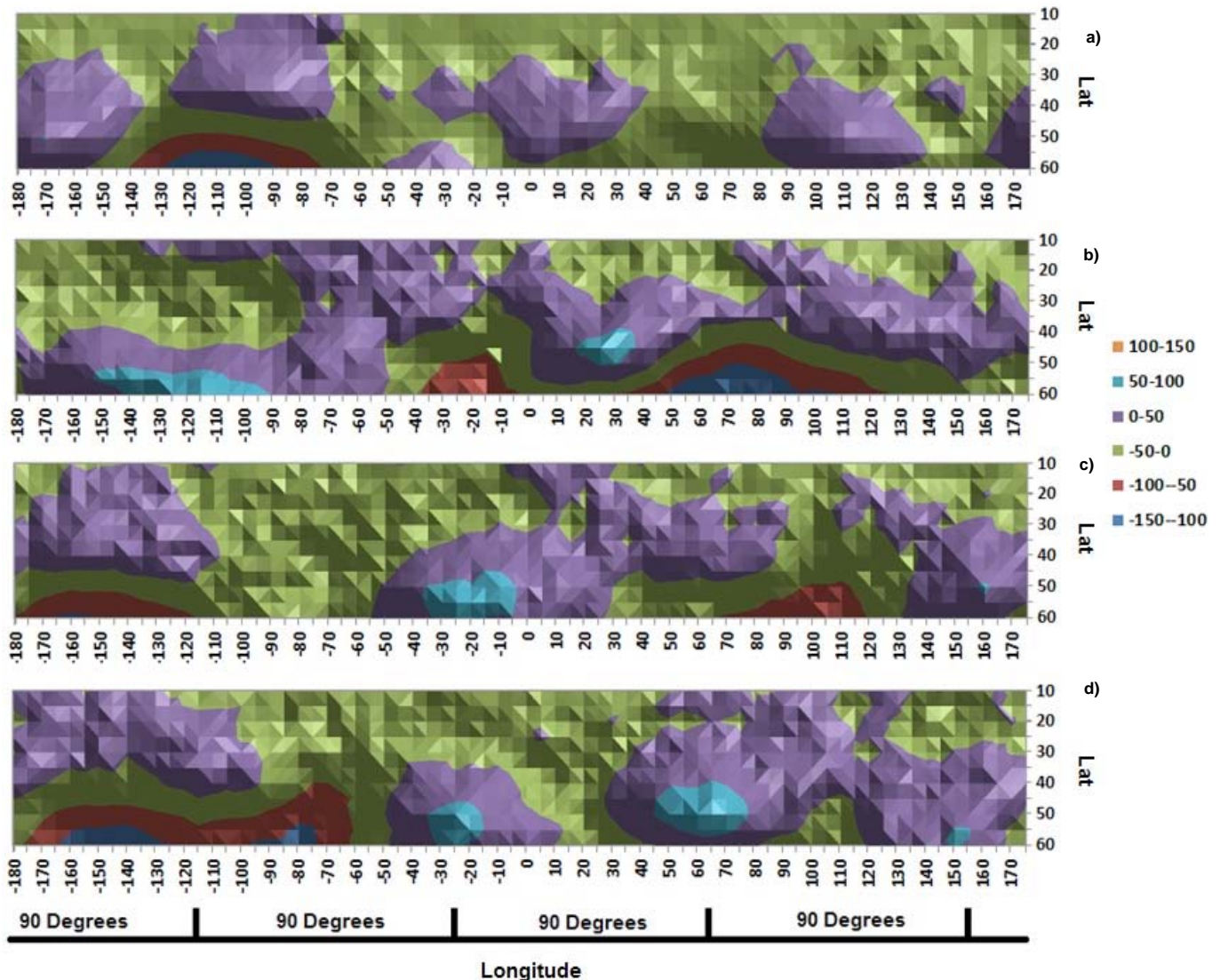


**Fig. (11).** (**a-d**) The shift-and-add maps of the Southern Hemisphere MSLP anomalies between the latitudes of 10 and 60 degrees between the years 1947 and 1970, for westerly drift rates of 0°, 10°, 20°, and 40° per year, respectively.

have been placed above the peaks of PSD at 20° and 40° per year in Fig. (**10**) in order to more precisely identify the actual circumnavigation times associated with these peaks. It is evident from a comparison between the PSD peaks and these lines that the circumnavigation times that best matches the positions of the two peaks are those of the 18.6 year lunar Draconic or the 18.0 year lunar Saros cycles.

Hence, Figs. (**10, 11a-d**) indicate that during the 1947 to 1970 climate epoch there are four extended features of higher-than-normal atmospheric pressure in the summer MSLP anomalies which are centred between 30 and 60° S and separated from each other by approximately 90 degrees in longitude (i.e. there is an N=4 pattern in the longitude profile).

In addition, these figures show that, over this climate epoch, these patterns are drifting in longitude at rates that produce circumnavigation times that match either the length of the 18.6 year lunar Draconic or the 18.0 year lunar Saros cycles.

### 4.2.2. The Southern Summer (DJF) Mean Sea-Surface Temperature Anomalies

Fig. (**12**) shows the relative PSD for features that have an N=4 pattern in the average longitudinal profile between 20° and 40° S, for the shift-and-add map of the summer mean SST anomaly, plotted against westerly longitudinal drift rate.

The westerly drift rates in Fig. (**12**) range from 0 to 90° of longitude per year, in steps of 5° per year.

Fig. (**12**) can be used to show the effect of the choice of normalization epoch has upon the PSD profile. Two PSD profiles are shown in Fig. (**12**), one for when the cell values for the SST anomaly data are normalized to their mean temperatures for the 1971 to 2000 climate epoch (the blue line), and the other for when the cell values for the SST anomaly data are normalized to their mean temperatures for the 1947 to 1970 climate epoch (the red line).

It is clear from a comparison of the two curves in Fig. (**12**) that choosing to normalize to an epoch that lies outside the range of the climate epoch under consideration (e.g. choosing to normalize to mean temperatures between 1971 to 2000 rather than 1947 to 1970) can introduce regional structure into the anomaly maps that has a N=4 pattern. In this case, the change in regional structure between the two climate epochs is most likely caused by changes in the levels of cloudiness over the Southern Oceans during the summer caused by variations in the strength of the semi-permanent high pressure cells embedded in the summer sub-tropic high pressure ridge. However, it is also clear from Fig. (**12**) that while a normalization to the 1971 to 2000 climate epoch introduces an N=4 pattern into the anomaly map for zero drift, these longitudinally fixed structures are quickly smeared out by the shift-and-add method for drift rates above 10° per year. Hence, the choice of normalization has a
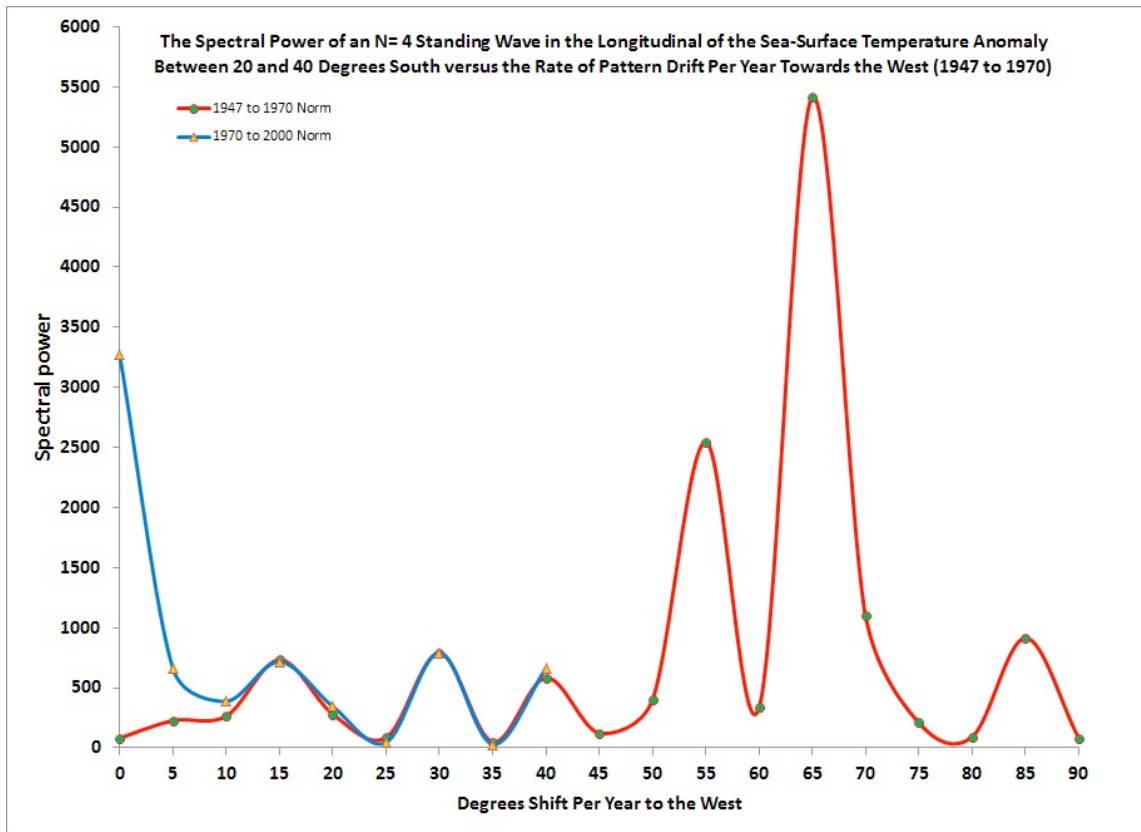


**Fig. (12).** The relative PSD for features that have an N=4 pattern in the average longitudinal profile between 20° and 40° S, for the shift-and-add map of the summer mean SST anomaly, plotted against westerly longitudinal drift rate. Two PSD profiles are shown in this figure, one for when the cell values for the SST anomaly data are normalized to their mean temperatures for the 1971 to 2000 climate epoch (the blue line), and the other for when the cell values for the SST anomaly data are normalized to their mean temperatures for the 1947 to 1970 climate epoch (the red line).

minimal effect upon the PSD profile that is produced by the shift-and-add method.

Fig. (**12**) shows that there are two drift rates that have prominent N=4 patterns in their summer SST anomaly profiles. The first is at a fixed westerly shift rate near 55° per year in longitude (time to circumnavigate the Earth ≈ 6.55 years), and the second is near 65° per year (circumnavigation time ≈ 5.54 years).

This interpretation is confirmed by Fig. (**13a-c**) which shows the shift-and-add maps of the Southern Hemisphere SST anomalies between the latitudes of 20-25° and 55-60° for three different drift rates. Fig. (**13a-c**) shows the maps for westerly drift rates of 0°, 55°, and 65° per year, respectively.

Fig. (**13a**) shows that if the 5° x 5° cells of SST data are normalized to their respective mean temperature values for the 1947 to 1970 climate epoch (the red line), there is no obvious longitudinal periodicity. This is in agreement with the low PSD seen at a zero drift rate in Fig. (**12**). Hence, the peaks in PSD seen in Fig. (**12**) cannot be the result of multi-annual modulations of the amplitude of a stationary N=4 pattern in the MSLP anomaly profiles). In contrast, both Fig. (**13b, c**, with respective westward drift rates of 55° and 65° per year), show strong features that exhibit an N=4 pattern straddling the Earth at a mean latitude of 30-35° S. Again, this is in agreement with the peaks in power spectral density that are seen at drift rates near 55° and 65° per year in Fig. (**12**).

It is important to note that if there were biennial oscillations of the amplitude of the N=4 patterns that were drifting at 55°, 65°, and 85° per year, you would expect to see similar peaks in the PSD in Fig. (**12**) at 10°, 20°, and 40° per year. The fact that you do not see these peaks in the PSD at these later drift rates indicates that the structures in the MSLP anomaly maps might be moving at 55°, 65°, and 85° per year. However, a more likely explanation is that the structures are in fact moving at 10°, 20°,

and 40° per year and that these moving structures are being modulated by a biennial oscillation in the phase (as opposed to the magnitude) of the N=4 pattern, such that the N=4 pattern is in-phase every two years, and 45° out-of-phase for the alternate years [see Appendix **A**].

## 5. DISCUSSION AND CONCLUSIONS

This paper sets out to look for large drifting structures in the MSLP and SST anomaly maps of the Southern Hemisphere that might be associated with the long-term lunar atmospheric tides.

The longitudinal shift-and-add method is used to search for N=4 standing wave-like spatial features in the summer (DJF) MSLP and SST anomaly maps. This method can be used to detect large spatial structures in the anomaly maps that are moving zonally (east-west) around the Earth at constant longitudinal drift rates.

The shift-and-add method is applied to the MSLP and SST anomaly maps for two adjacent climate epochs, each of which lasts for 24 years. The first climate epoch is from 1947 to 1970, while the second is from 1971 to 1994.

### 5.1. The Identification of Large Structures Drifting Through the Summer MSLP Anomaly Maps

When the shift-and-add method is applied to the Summer (DJF) MSLP anomaly maps between 1947 and 1994 the stacked anomaly maps show that for most of this period:

a.  there are longitudinal N=4 patterns in the MSLP anomalies that straddled the Earth between 35° and 55° S.

b.  the standing wave-like patterns consisted of four extended regions of abnormal atmospheric pressure that can be as large as 20° (latitude) × 30° (longitude) in size, that are separated from each other by ~ 90° in longitude.
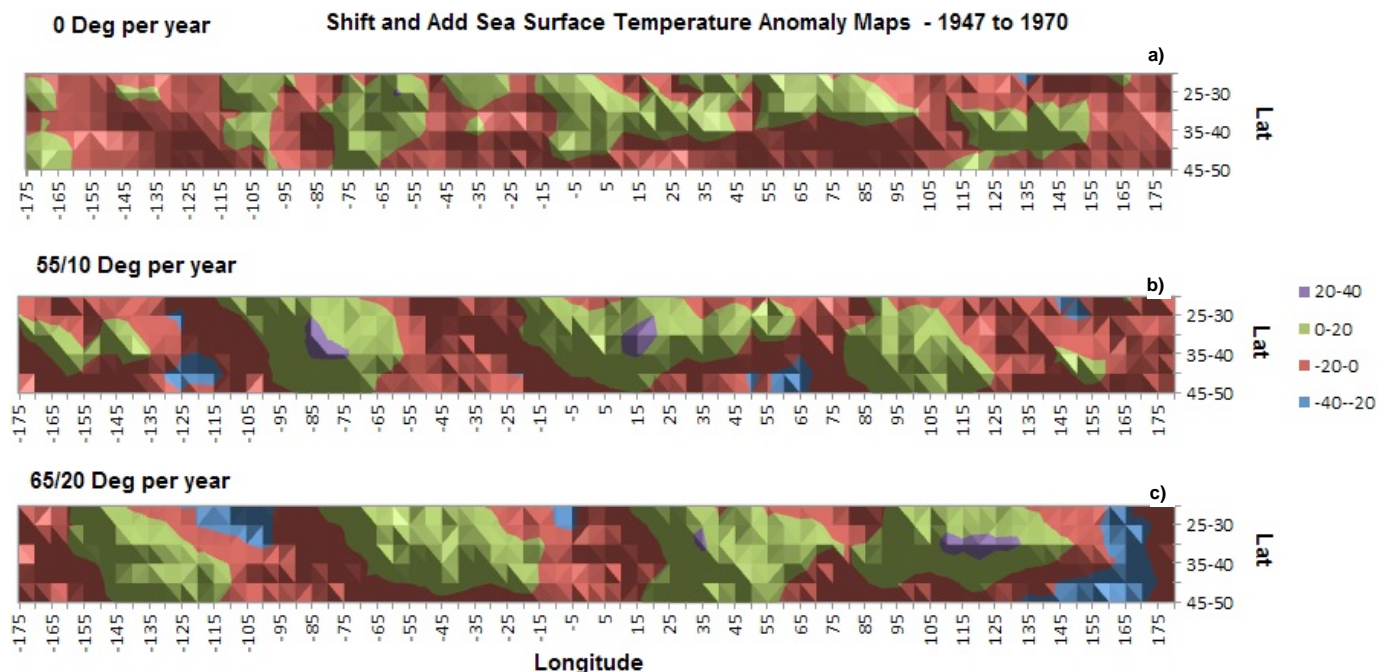


**Fig. (13).** (**a-c**) The shift-and-add maps of the Southern Hemisphere SST anomalies between the latitudes of 20-25° and 55-60° for westerly drift rates of 0°, 55°, and 65° per year, respectively.

c.    the N=4 patterns are drifting towards the west at constant rates of 10°, 20° and 40° per year, corresponding to circumnavigation times of ~ 36, 18 and 9 years, respectively.

d.    the circumnavigation times of the N=4 pattern most closely match the length of multiples and sub-multiples of the 18.6 year lunar Draconic or the 18.0 year lunar Saros cycles.

The shift-and-add method also shows that there is a triennial oscillation in the strength of the drifting standing wave-like pattern during the first climate epoch between 1947 and 1970, and a biennial oscillation in the strength during the second climate epoch between 1971 and 1994.

The triennial oscillations in the strength of the standing wave-like features in the first climate epoch means that the shift-and-add method cannot distinguish between features that are drifting towards the west at 10° and 20° per year from those that are drifting to the west at 40° and 50° per year, respectively.

In like manner, biennial oscillations in the strength of the standing wave-like features in the second climate epoch, means that the shift-and-add method cannot distinguish between features drifting towards the west at 10° per year from those that are drifting to the west at 55° per year.

Finally, the shift-and-add method shows that during the first climate epoch between 1947 and 1970 the pressure of the four extended regions is higher-than-normal, while the pressure of these regions is lower-than-normal during the second climate epoch between 1971 and 1994.

This means that once every 4.5 years during the first climate epoch, the four main regions of enhanced atmospheric pressure passed over the four large semi-permanent high pressure systems in the summer sub-tropical high pressure ridge. When this occurs, a large moving region of enhanced atmospheric pressure increases the pressure of the South Pacific sub-tropical high hovering over Easter Island, causing a temporary strengthening of the East-Pacific Trade Winds. This may have led to conditions that favor the onset of La Nina events over El Nino events throughout the first climate.

It also means that once every 4.5 years during the second climate epoch, the four main regions of reduced atmospheric pressure passed over the four large semi-permanent high pressure systems in the summer sub-tropical high pressure ridge. When this occurs, a large moving region of reduced atmospheric pressure decreases the pressure of the South Pacific sub-tropical high hovering over Easter Island, causing a temporary reduction in the strength of the East-Pacific trade winds. This may have led to conditions that favor the onset of El Nino events over La Nina events throughout the second climate.

## 5.2. The Identification of Large Structures Drifting Through the Summer SST Anomaly Maps

When the shift-and-add method is applied to the Summer (DJF) SST anomaly maps for the period between 1947 and 1994 the stacked anomaly maps show that:

a.    there are longitudinal N=4 patterns in the SST anomalies that straddled the Earth between 25-30° and 45-50° S.

b.    the standing wave-like patterns consisted of four extended regions of above normal SST that can be as large as 20° (latitude) × 30° – 40° (longitude) in size, that are separated from each other by ~ 90° in longitude.

c.    there are no strong biennial or triennial modulations in the amplitude of the drifting standing wave-like patterns in the SST anomalies.

The main differences between the two climate epochs are that:

a.    during the first climate epoch, the structures that are drifting at 55°, 65°, and 85° per year are being modulated by a biennial oscillation in the phase (as opposed to the magnitude) of the N=4 pattern, such that the N=4 pattern is in-phase every two years, and 45° out-of-phase for the alternate years. This means that the structures are actually moving towards the west at 10°, 20°, and 40° per year (corresponding to circumnavigation times of 36, 18 and 9 years, respectively). The circumnavigation times for the N=4 patterns in the SST anomalies indicate that they are related to lunar atmospheric tides that are being driven by either the 18.03 (tropical) year lunar Saros cycle or the 18.60 (tropical) year lunar draconic cycle.

b.    during the second climate epoch, the most prominent N=4 patterns are drifting towards the west at constant rates near 17.5° and 35° per year (corresponding to circumnavigation times of 20.6 and 10.3 years, respectively). In this case, the circumnavigation times of the N=4 patterns in the SST anomalies closely match the length of the 20.3 year lunar Perigee-Syzygy cycle and its first sub-multiple.

## 5.3. A Possible Explanation for the Drifting Structures in the MSLP and SST Anomaly Maps

### 5.3.1. The 1971 to 1994 Climate Epoch

In this climate epoch there are N=4 patterns in the MSLP anomaly profiles that have circumnavigation times that closely match the lengths of the 18.03 (tropical) year lunar Saros cycle or the 18.60 (tropical) year lunar draconic cycle. In addition, there are N=4 patterns in the SST anomaly profiles that have circumnavigation times that closely match the 20.294 (tropical) year Perigee-Syzygy lunar cycle.

The fact that standing wave-like patterns in the MSLP anomalies and the SST anomalies are moving around the Earth at different rates and that the moving patterns in the MSLP anomalies appear around 1971 and then disappear roughly 24 years later around 1994, indicate that both patterns may only become visible because of a process of mutual pattern reinforcement.

If you have a N=4 pattern in the MSLP anomalies that is moving towards the west at 17.74° per year (corresponding to a circumnavigation time of 20.294 years), it will drift out of phase with (i.e. be 45° in longitude ahead of) an N=4

pattern in the SST anomalies that is moving towards the west at 19.97°/19.35° per year (corresponding to circumnavigation times of 18.03/18.60 years) in 20.20/27.86 years, respectively. So, on average, one pattern will drift-in and then out-of-phase with the other over a period of roughly 24 years, in good agreement with the time of visibility of the moving patterns in the MSLP and SST anomalies maps.

Hence, the observational evidence suggests that we are seeing a process that is result of a mutual reinforcement of the lunar Draconic Cycle and the lunar Perigee-Syzygy cycle.

### 5.3.2. The 1947 to 1970 Climate Epoch

In this climate epoch there are N=4 patterns in both the MSLP and SST anomaly profiles that have circumnavigation times that closely match the lengths of the 18.03 (tropical) year lunar Saros cycle or the 18.60 (tropical) year lunar Draconic cycle. There is no evidence of patterns in the SST that have circumnavigation times that match the length of the Perigee-Syzygy cycle.

The fact that standing wave-like patterns in the MSLP anomalies and the SST anomalies are both moving around the Earth at the same drift rates and that these drift rates closely match the lengths of the lunar Saros or Draconic cycles, indicates that we are seeing a process where the tidal effects of the lunar Draconic cycle are no longer being reinforced by the lunar Perigee-Syzygy cycle.

### 5.3.3. The 31/62/93/186 Year Lunar Tidal Cycle

All of the data being analyzed in this study is subject to an annual aliasing, since it is limited to the three months of the Southern Hemisphere's summer. In essence, this means that we are seeing the effects of lunar tidal forces upon the Earth's atmosphere and oceans that are being sampled at the same point in the Earth's orbit about the Sun (in this case, from roughly one month before to two months after perihelion on January 3rd - Standish and Williams [18]).

There is one lunar tidal cycle that naturally peaks in strength at the same point in the Earth's orbit (i.e. in the same season) that is produced by the long-term interaction between the Perigee-Syzygy cycle (Treloar [19]), the Draconic lunar tidal cycles (Baart *et al.* [20]) and perihelion. This is the 31/62/93/186 year lunar tidal cycle.

We propose that it is this tidal cycle that is responsible for producing the mutually reinforcing N=4 propagating standing wave-like pattern that are seen in the MSLP and SST anomaly maps of the atmosphere and oceans of the Southern Hemisphere between 1971 and 1994.

The Line-of-Apse of the lunar orbit must precess seven times around the Earth with respect to the stars (i.e. 7 x 8.8506 = 61.954 tropical years) before it closely re-aligns with the Earth-Sun line at the time of perihelion. In addition, a New Moon at closest perigee re-aligns itself to the Earth-Sun line at perihelion once every three Perigee-Syzygy cycles plus one Full Moon Cycle (i.e. [3 x 20.2937] + 1.1274 = 62.0085 tropical years) or 55 Full Moon Cycles (one FMC = the beat period for the lunar synodic and lunar anomalistic months – Chapront-Touzé and Chapront [21]). This phenomenon is the result of the fact that 767 lunar synodic

months (= 767 x 29.530589 = 22649.9617 days) is almost the same length of time as 822 lunar anomalistic months (= 822 x 27.554550 = 22649.8340 days), and both of these are within two days of 55 Full Moon Cycles (= 55 x 411.784430 = 22648.1437 days). Hence, if you start out with a New Moon at closest perigee at or near the time of perihelion, you will get a Full Moon at closest perigee, on roughly the same day 31 years later, and a New Moon at closest perigee, on roughly the same day, 62 years after the starting date.

The Line-of-Nodes of the lunar orbit must precess five times around the Earth with respect to the stars (i.e. 5 x 18.5999 = 92.9996 tropical years) before it closely re-aligns with Earth-Sun line at perihelion. This means that if you start out with a New Moon at or near the time of perihelion that is close to one of the nodes of the lunar orbit and at perigee, 93 tropical years later you will have a Full Moon that is close to the same node and at perigee on roughly the same day of the year. This is true because 1150.5 lunar synodic months (= 33974.9425 days = 93.020 tropical years) is almost the same length as 1233 lunar anomalistic months (= 33974.7600 days) and 1248.5 draconic months (=33974.4577 days). [N.B. The full tidal cycle is actually 186 years long since it takes this long for the Moon to return to a New Moon phase at a time when it returns to the same node, at perigee, and at perihelion].

In order to get a sense of the times when the lunar Perigee-Syzygy cycle and the lunar Draconic Cycle mutually reinforced each other, curves are plotted in Fig. (**14**) that indicate the strength of alignment between the two cycles between the years 1857 and 2024. The blue curve in Fig. (**14**) shows the angle between the line-of-nodes of the lunar orbit and the Earth-Sun line at the time of Perihelion (θ). The curve is derived in such a way as to highlight the southern summers where there is close alignment. This is done by plotting the function 1/(1+θ).

Similarly, the brown curve in Fig. (**14**) shows the angle between the line-of-apse of the lunar orbit and the Earth-Sun line at the time of perihelion (φ) plotted as the function −1/(1+φ).

The functions represented by the blue and brown curves in Fig. (**14**) are used to generate the red curve in this figure. The red curve is an alignment index that is designed to represent the level of reinforcement of the Draconic tidal cycle by the Perigee-Syzygy tidal cycle. This is done by plotting the values of the blue curve at times when there is a close alignment of the line-of-apse and the Earth-Sun line at perihelion (i.e. when φ ≤ 16°). The red curve shows that are two epochs, each lasting about 37-38 years, where there is a strong mutual reinforcement of the Draconic tidal cycle by the Perigee-Syzygy tidal cycle. Individual peaks in the mutual reinforcement occur roughly once every 9.3 years and comparable peaks in the two climate epochs are separated from each other by 93 years.

Hence, if the proposed mutual reinforcement model is correct, it would predict that there should be N=4 standing wave-like features in the Southern Hemisphere's MSLP and SST anomaly maps, similar to those seen in the second climate epoch (i.e. from 1971 to 1994), between about 1878 and 1901.
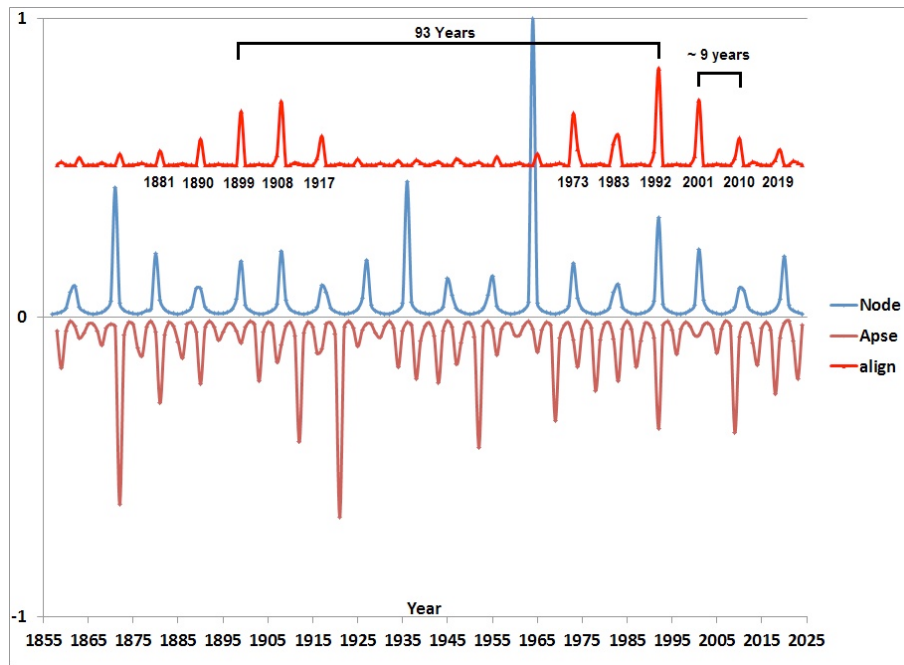
**Fig. (14). Blue curve:** The angle between the line-of-nodes of the lunar orbit and the Earth-Sun line at the time of Perihelion ($\theta$) is plotted as a function $1/(1+\theta)$ between the years 1857 and 2024, in order to highlight the years in which these two axes are is close alignment. **Brown curve:** The angle between the line-of-apse of the lunar orbit and the Earth-Sun line at the time of perihelion ($\varphi$) plotted as the function $-1/(1+\varphi)$, in order to highlight the years in which these two axes are is close alignment. **Red curve:** This is an alignment index that is designed to represent the level of reinforcement of the Draconic tidal cycle by the Perigee-Syzygy tidal cycle. This is done by plotting the values of the blue curve at times when there is a close alignment of the line-of-apse and the Earth-Sun line at perihelion (i.e. when $\varphi \leq 16°$).

Unfortunately, the quality of the MSLP and SST data in the late 19th and early 20th centuries is not of a high enough standard to be able to fairly test this prediction. However, there is some circumstantial evidence that when the Draconic tidal cycle is predicted to be mutually enhanced by the Perigee-Syzygy tidal cycle there are observable effects upon the climate variables in the South Eastern part of Australia. Fig. (**15**) shows the median summer time (December 1st to March 15th) maximum temperature anomaly (The Australian BOM High Quality Data Sets 2010 [22]), averaged for the cities of Melbourne (1857 to 2009 – Melbourne Regional Office – Site Number: 086071) and Adelaide (1879 to 2009 – Adelaide West Terrace – Site Number 023000 combined with Adelaide Kent Town – Site Number 023090), Australia, between 1857 and 2009 (blue curve). Superimposed on Fig. (**15**) is the alignment index curve from Fig. (**14**, red line). A
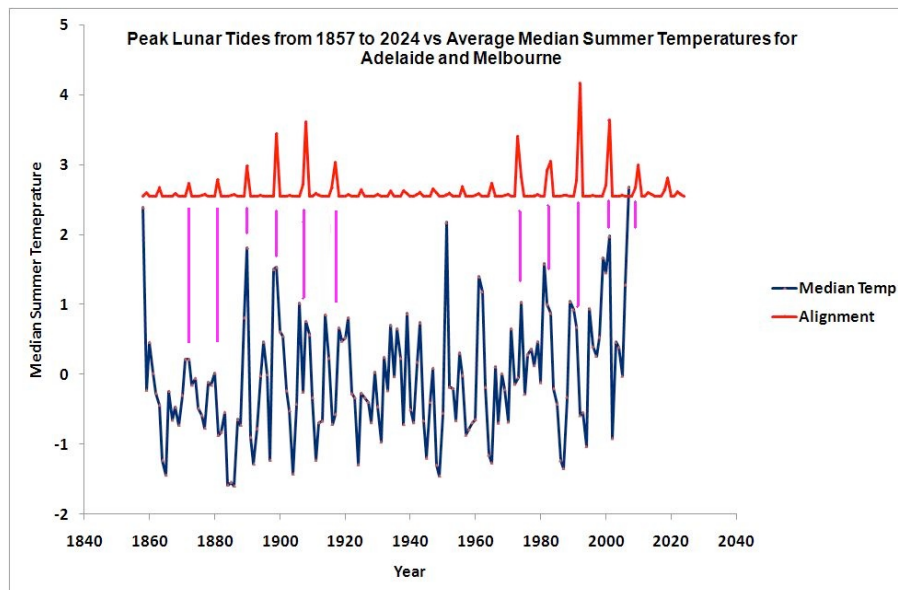


**Fig. (15).** The median summer time (December 1st to March 15th) maximum temperature, averaged for the cities of Melbourne and Adelaide, Australia, between 1856 and 2010 (blue curve). The alignment index curve from Fig. (**13**) is superimposed on this figure (red line).

comparison between these two curves reveals that on almost every occasion where there has been a strong alignment between the Draconic and Perigee-Syzygy tidal cycles, there has been a noticeable increase in the median maximum summer-time temperature, averaged for the cities of Melbourne and Adelaide. Hence, if the mutual reinforcing tidal model is correct then this data set would predict that the median maximum summer time temperatures in Melbourne and Adelaide should be noticeably above normal during southern summer of 2018/19.

## CONFLICT OF INTEREST

The authors confirm that this article content has no conflict of interest.

## ACKNOWLEDGEMENTS

## APPENDIX A

There is an ambiguity in the longitudinal drift direction of N=4 patterns in the anomaly maps when they are analyzed with the shift-and-add method. The method gives the same result for standing wave-like patterns that are moving towards the west at $X°$ per year as it does for standing wave-like patterns moving towards the east at $90 - X°$. This ambiguity must be resolved.

Fig. (**A1**) shows the average MSLP anomaly between the latitudes of 20° S and 50° S, as a function of longitude, for

the years 1974 and 1997. Both of these profiles show the classic N=4 longitudinal pattern. Fig. (**A2**) shows the cross-correlation functions derived using the XCORR function (DADisp 2002 [23]) for the 1974 and 1997 MSLP anomaly profiles that result from using the 1974 MSLP anomaly profile as the template. Cross-correlation functions like that shown in Fig. (**A2**) can be used to measure the annual longitudinal lag (or drift) of the N=4 pattern that is seen in a given MSLP anomaly profile compared to a profile that is seen in a template year.

The map on the right-hand side of Fig. (**A3a**) displays all of the cross-correlation functions using 1964 as a template for each year between 1971 and 2009, stacked together. This map is designed to show the evolution of the annual longitudinal lag of the MSLP anomaly profiles over second climate epoch. The map is reproduced on the left-hand side of Fig. (**A3a**).

The map on the left-hand side of Fig. (**A3a**) reveals that the N=4 pattern is moving towards the east between 1971 and 1976, towards the west between 1977 and 1986, and then possibly back towards the east again between 1987 and 1991. In fact, the change in drift can be fitted by a sinusoid with a period of ~ 19 – 20 years. However, there is some uncertainty about the direction of drift after 1987, and it is possible that the westerly drift might continue until at least 1994 [N.B. Interestingly, Fig. (**A3a**) indicates that there is little or no drift in the standing wave-like pattern in the MSLP anomaly profiles after 1994].
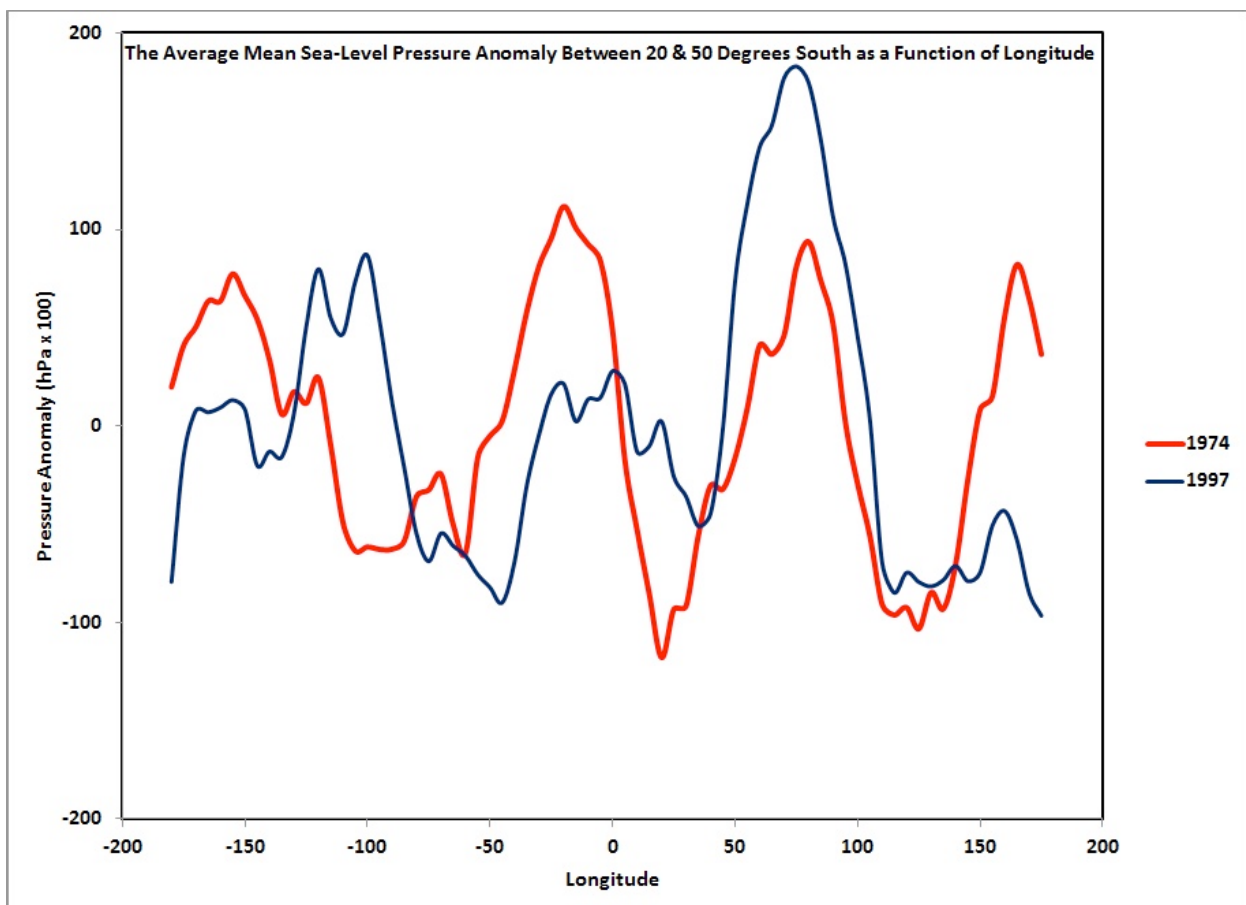


**Fig. (A1).** The average MSLP anomaly between the latitudes of 20° S and 50° S, as a function of longitude, for the years 1974 and 1997.
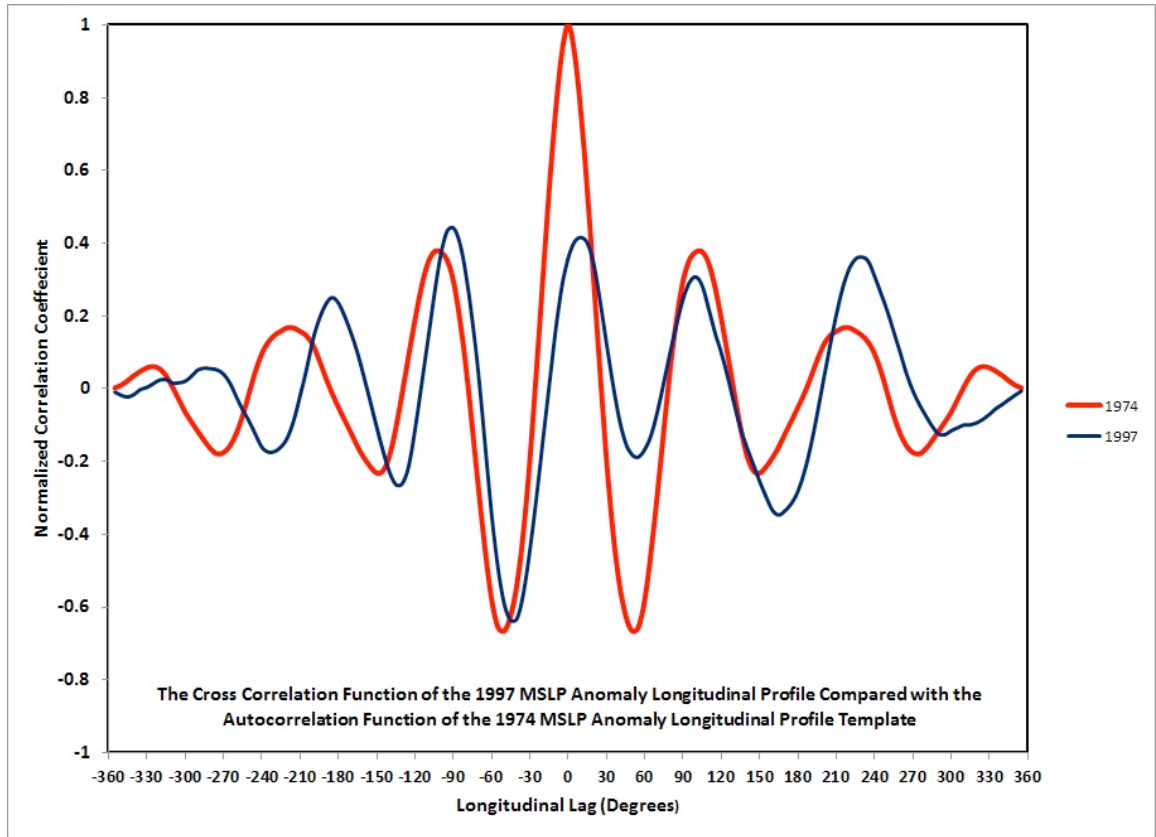
**Fig. (A2).** The cross-correlation functions for the 1974 and 1997 MSLP anomaly profiles that result from using the 1974 MSLP anomaly profile as the template.
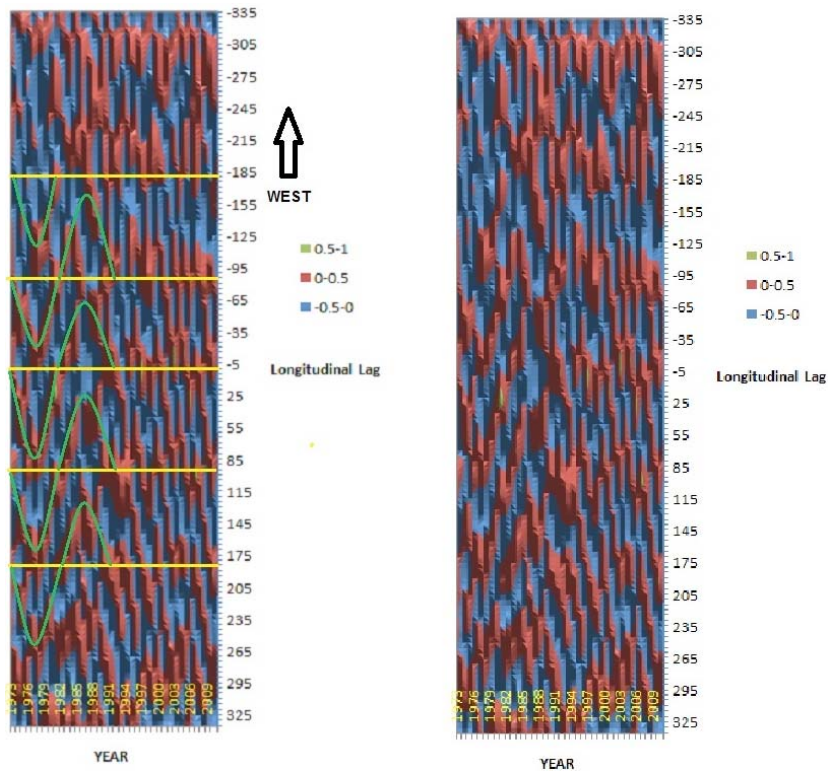


**Fig. (A3a).** The map on the right-hand side of Fig. (**A3a**) displays the cross-correlation functions, for all years from 1971 to 2009, which use the 1964 profile as a template, stacked together to form a map. This map is reproduced on the left-hand side of Fig. (**A3a**) to show that the N=4 pattern is moving towards the west over most of the period between 1971 and 1994.
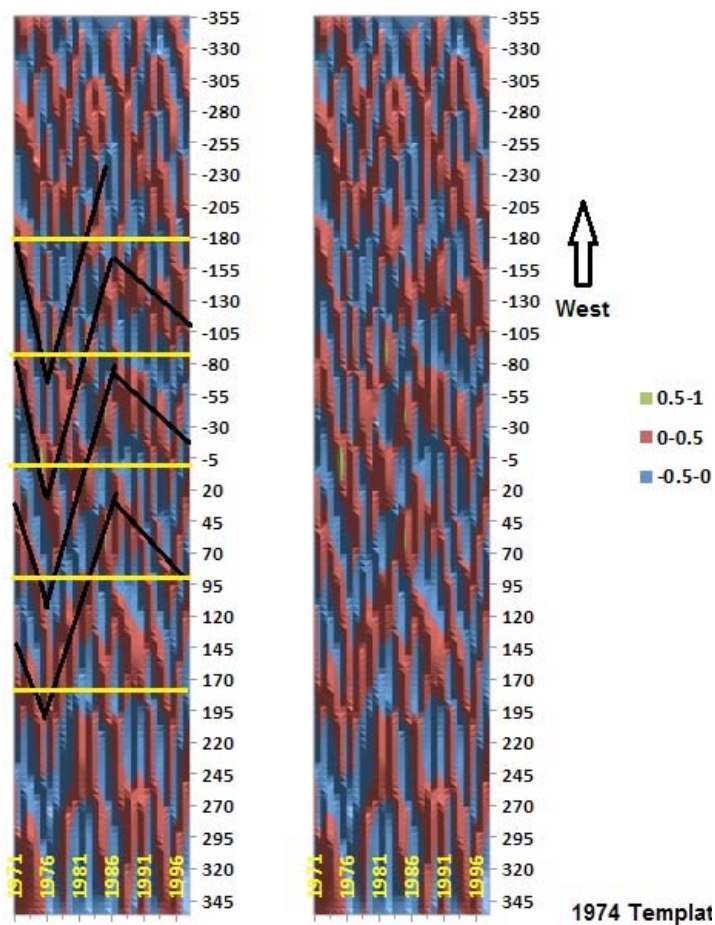
**Fig. (A3b).** This is the corresponding cross-correlation map to that shown in Fig. (**A3a**), which using 1974 as a template, for all years from 1971 and 1998, stacked together to form a map. This map is included to show the effects of changing the template year.

The map on the right hand side of Fig. (**A3b**) displays all of the cross-correlation functions using 1974 as a template for each year between 1971 and 1998, stacked together. This map is included to show the effects of changing the template year. Again we see the drift to the east up until 1976, changing over to a westerly drift between 1977 and 1986.

Both Fig. (**A3a, b**) show that at least half, and possibly more of the longitudinal drift between 1971 and 1994 is towards the west, confirming the choice of direction used in Fig. (**4**).

Fig. (**A4a**) shows the average SST anomaly between the latitudes of 20° S and 50° S, as a function of longitude, for
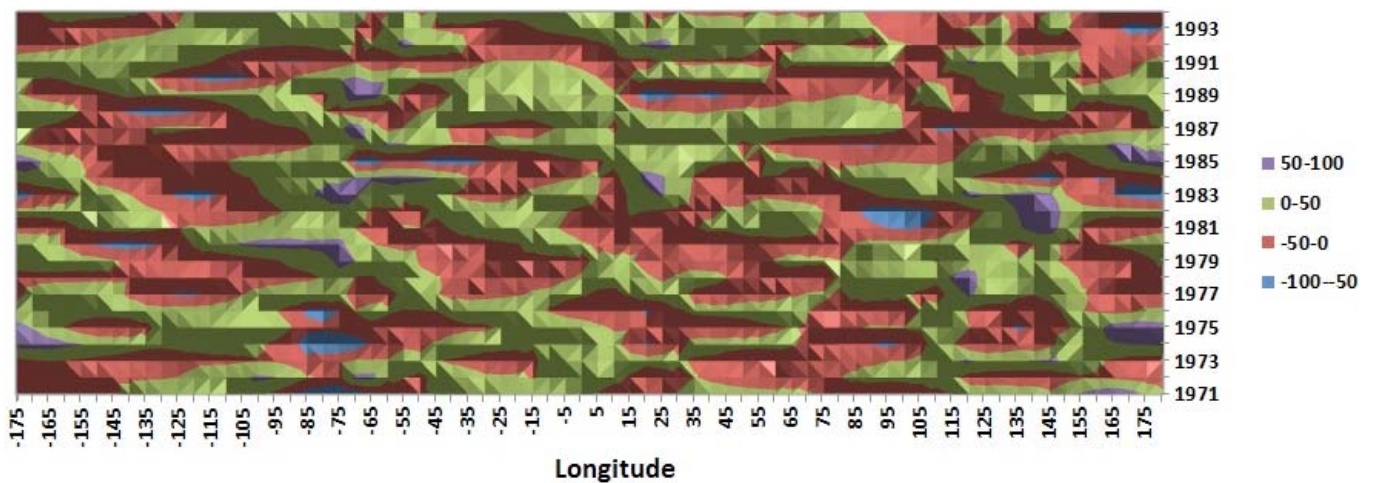


**Fig. (A4a).** Shows the average SST anomaly between the latitudes of 20° S and 50° S, as a function of longitude, for each of the years between 1971 and 1994. These SST anomaly profiles have been stacked to form a map that shows the evolution of these profiles over the second climate epoch.
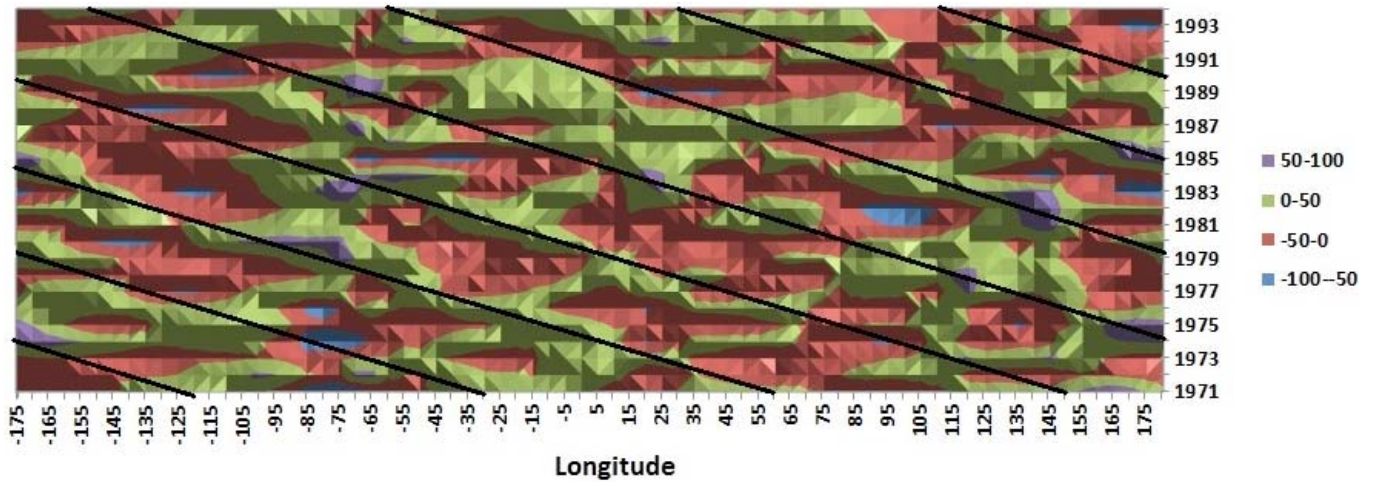
**Fig. (A4b).** This is a re-plotted in Fig. (**A4b**) with black lines superimposed on top that show how the four main regions of warmer-than-normal sea-surface temperature in the 1971 longitudinal profile would move if they were drifting towards the west at 17.5° per year.

each of the years between 1971 and 1994. These SST anomaly profiles have been stacked to form a map that shows the evolution of these profiles over the second climate epoch. Fig. (**A4a**) is re-plotted in Fig. (**A4b**) with black lines superimposed on top that show how the four main regions of warmer-than-normal sea-surface temperature in the 1971

longitudinal profile would move if they were drifting towards the west at 17.5° per year. It is evident from Fig. (**A4b**) that there is a tendency for the SST anomaly data to fall along the lines that correspond to the indicated drift rate. Support for this claim is provided by Fig. (**A4c**).
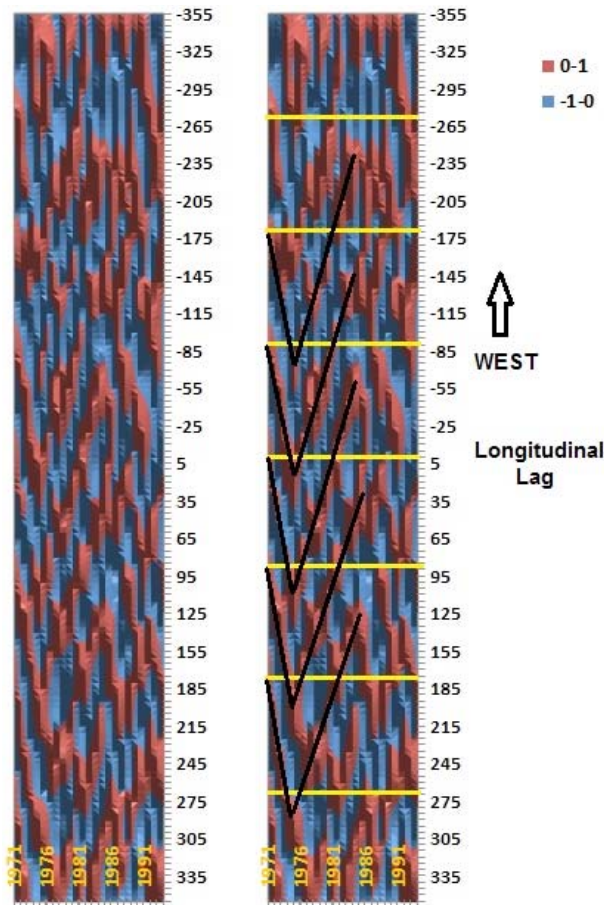


**Fig. (A4c).** The map on the right-hand side of this figure displays the stacked cross-correlation functions of the average SST anomaly longitudinal profiles between latitudes 20° S and 50° S, for all years from 1971 to 1994. (N.B. The template year is 1973). This map is reproduced on the left-hand side of this figure to show that the N=4 pattern is moving towards the west over most of the period between 1971 and 1994.

This figure reveals that there is an N=4 pattern that is moving towards the east between 1971 and 1975, and then to the west between 1977 and 1986. What is important, however, is that the longitudinal drift of the N=4 patterns in the SST anomaly profiles between 1970 and 1994 is predominantly towards the west, confirming the choice of direction in Fig. (**8**).

Finally, the map on the left-hand side of Fig. (**A5**) displays all of the cross-correlation functions using the 1950 profile as a template for each year between 1947 and 1970, stacked together. This map is designed to show the evolution of the annual longitudinal lag of the SST anomaly profiles over the first climate epoch.

The relative PSD plot for N=4 patterns in the SST anomaly maps in the first climate epoch (see Fig. **12**) showed that there were structures moving at drift rates of 55°, 65°, and 85° per year. However, it was claimed that these patterns were in fact moving at 10°, 20°, and 40° per year because they were being modulated by a biennial oscillation in the phase (as opposed to the magnitude) of the N=4 pattern. The modulations were such that the N=4 pattern were in-phase every second year, and 45° out-of-phase for the alternate years.

Proof of this claim is provided in Fig. (**A5**). The second map from the left in this figure shows the cross-correlation functions (template: 1950) for all of the even years between 1947 and 1970. The cross-correlation functions for the odd years have been set to zero in this map. Similarly, the fourth map from the left in Fig. (**A5**) shows the cross-correlation functions (template: 1950) for all of the odd years over the same time frame. In like manner, the cross-correlation functions for the even years have been set to zero in this map.

The second and fourth maps from the left in A5 are reproduced in the third and fifth maps, respectively. These latter maps show that the N=4 pattern is being modulated by a biennial oscillation in phase (as opposed to the magnitude) every second year, such that the pattern moves in- and out-of- phase by roughly 45° once every two years, as claimed.

**APPENDIX B**

This paper uses simple anomalies, rather than standardized anomalies, because of concerns about the effects that the missing standard deviation values has upon the quality of the data. However, it is essential that we attempt to estimate the statistical significance of the N=4
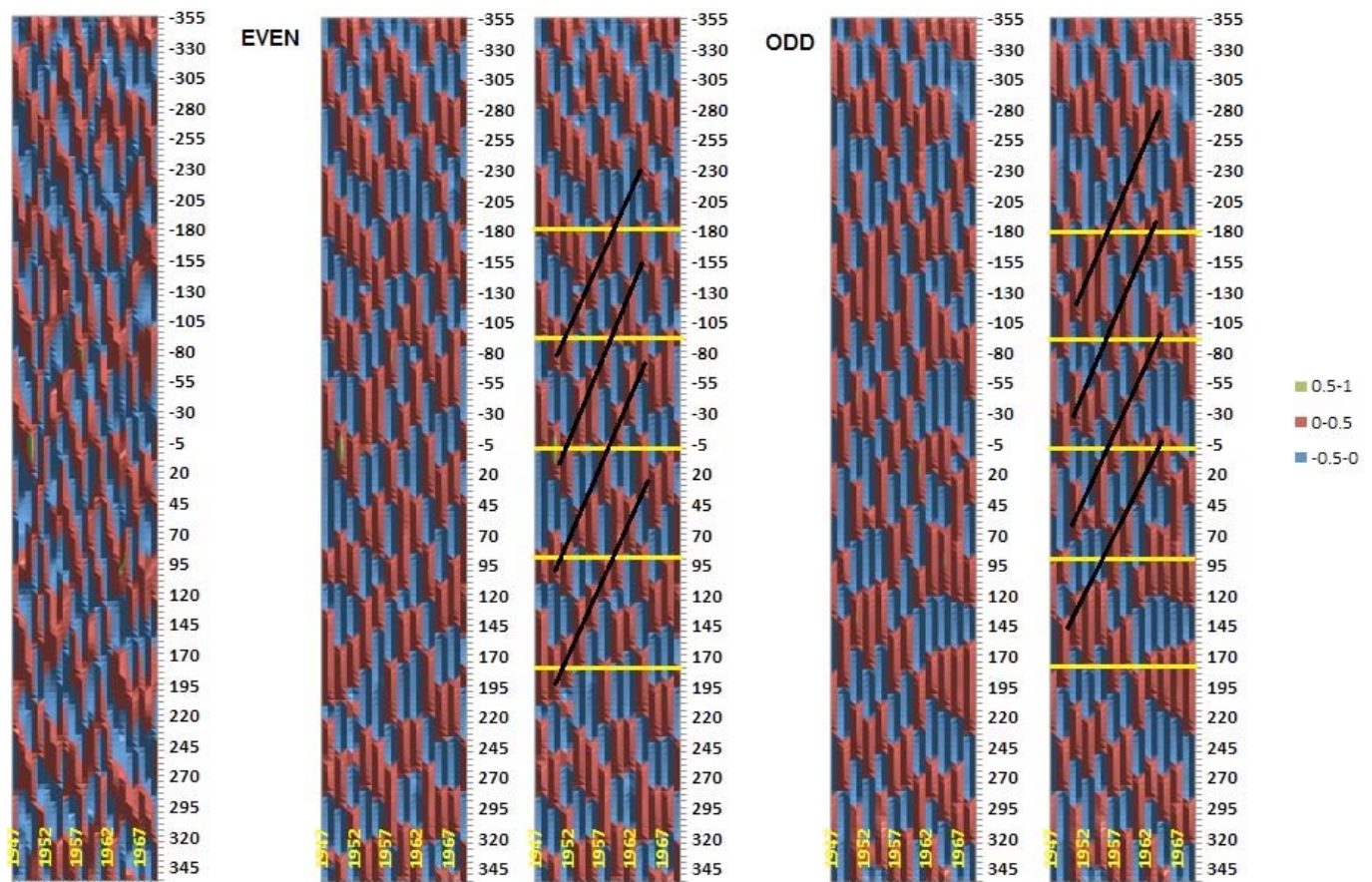


**Fig. (A5).** The map on the left-hand side of this figure displays all of the cross-correlation functions (template: 1950) for each year between 1947 and 1970, stacked together. This map is designed to show the evolution of the annual longitudinal lag of the SST anomaly profiles over the first climate epoch. The second map from the left in this figure shows the cross-correlation functions (template: 1950) for all of the even years between 1947 and 1970. The fourth map from the left shows the cross-correlation functions (template: 1950) for all of the odd years over the same time frame. The second and fourth maps from the left are reproduced in the third and fifth maps, respectively. These latter maps show that the N=4 pattern is being modulated by a biennial oscillation in phase (as opposed to the magnitude) every second year, such that the pattern moves in- and out-of- phase by roughly 45° once every two years.
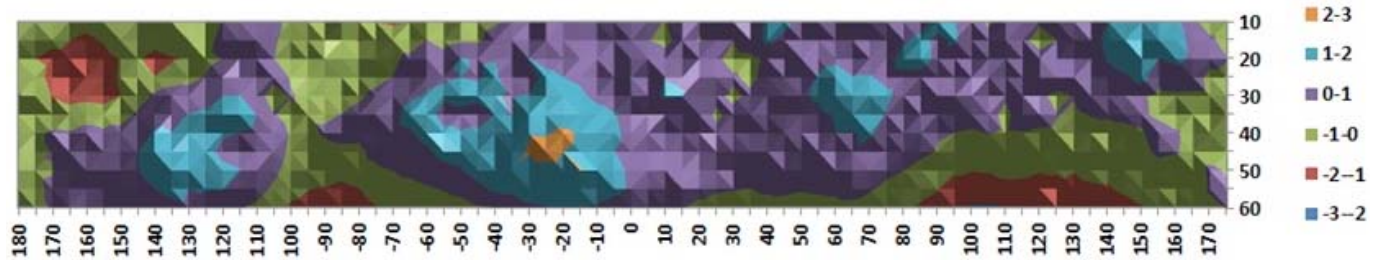
**Fig. (B1a).** The standardized MSLP anomaly map for a westerly drift rate of 20° per year over the second climate epoch. The N=4 pattern is clearly visible in this stacked shift-and-add map, although at the 5 × 5 degree bin resolution, only the strongest peak at a longitude of 25° W is statistically significant.
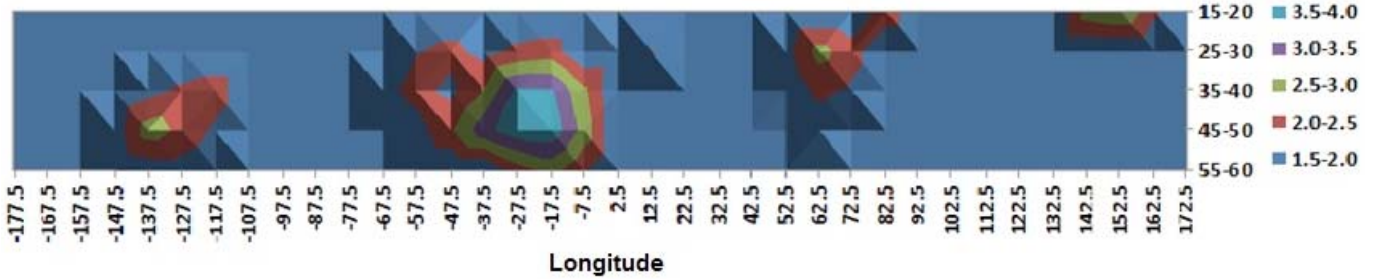


**Fig. (B1b).** The same standardized MSLP anomaly map as Fig. (**B1a**), after it has been double binned in both latitude and longitude. In this figure, all points with values that are at or above the brown level are statistically significant (i.e. the probability that it these value could have been produced by noise by chance p < 0.05).

patterns that we are detecting in the stacked MSLP anomaly maps.

Firstly, the gridded standard deviation data was broken up into a set of individual longitudinal profiles. Each of these profiles was formed by grouping together all of the cells that shared the same latitude and then arranging them in order of increasing longitude from 180° W to 175° E.

Secondly, a crude boot-strap method was used to fill-in the missing standard deviation values. This method consisted of temporarily setting the missing standard deviation values [i.e. those flagged with a value of -9999] to zero and then replacing these zero values with the mean value of their particular longitudinal profile. This crude method turns out to very effective way to fill in missing standard deviation values for the simple reason that there is large systematic increase the standard deviation of the MSLP with increasing latitude. Its only failing, is that it slightly underestimates the missing standard deviation values south of 45° S because of the increasing number of zero values in a given longitudinal profile.

Thirdly, the variance (i.e. the square of the standard deviations) of MSLP anomalies were calculated for each of the 5 × 5 degree bins for December, January and February of each year between 1971 and 1994.

The shift and add method was applied separately to the variance maps for December, January and February, before they were combined into a stacked variance map averaged over the three southern summer months. Finally, the combined DJF stacked variance map was used to determine the standardized MSLP anomaly for each of the 5 × 5 degree bins in the stacked shift- and-add map.

Fig. (**B1a**) shows the standardized anomaly map for a drift rate of 20° per year in a westerly direction [compare this with non-standardized anomaly map in Fig. (**6c**)]. The N=4 pattern is clearly visible in this stacked shift-and-add map, although at the 5 × 5 degree bin resolution, only the strongest peak, at a longitude of 25° W, has a value that is statistically significant (i.e. it exceeds 2σ so that the probability that it this value could have been produced by the noise by chance p < 0.05). However, Fig. (**B1b**) shows the same standardized anomaly map after it has been double binned in both latitude and longitude. In this figure, all points with values that are at or above the brown level are statistically significant (i.e. the probability that it these value could have been produced by noise by chance p < 0.05), proving that the N=4 pattern in the stacked shift-and-add MSLP anomaly map is indeed real.

## REFERENCES

[1]     Sidorenkov NS. Chandler Wobble of the poles as part of the nutation of the Atmosphere, Ocean, Earth system. Astron Rep 2000; 44 (6): 414-9.

[2]     Sidorenkov NS. Excitation mechanism of Chandler polar motion. Astron J 1992; 69 (4): 905-9.

[3]     Sidorenkov N S. The effect of the El Nino Southern oscillation on the excitation of the Chandler motion of the Earth's pole. Astron Rep 1997; 41(5): 705-8.

[4]     Sidorenkov NS. Physics of the Earth's rotation instabilities. Astron Astrophys Transact 2005; 24(5): 425-39.

[5]     Li G. 27.3-day and 13.6-day atmospheric tide and lunar forcing on atmospheric circulation. Adv Atmos Sci 2005; 22(3): 359-74.

[6]     Li G, Zong H. 27.3-day and 13.6-day atmospheric tide. Sci China (D) 2007; 50(9): 1380-95.

[7]     Li G, Zong H, Zhang Q. 27.3-day and average 13.6-day periodic oscillations in the earth's rotation rate and atmospheric pressure fields due to celestial gravitation forcing. Adv Atmos Sci 2011; 28(1): 45-58.

[8]     Krahenbuhl DS, Pace MB, Cerveny RS, Balling Jr RC. Monthly lunar declination extremes' influence on tropospheric circulation patterns. J Geophys Res 2011; 116: D23121- 6.

[9]     Wilson IRG. Lunar tides and the long-term variation of the peak latitude anomaly of the summer Sub-Tropical High Pressure Ridge over Eastern Australia. 2012. Open Atmos Sci J 2012; 6: 49-60.

[10] NOAA. Available at: ftp://public.sos.noaa.gov/oceans/SST_1980-1 999/2048_rolled/cyl_1981_01_25.jpg [Accessed: September 2012].

[11] Allan R.J. and Ansell T., A new globally complete monthly historical gridded mean sea level pressure dataset (HadSLP2): 1850-2004. J Clim 2006; 19: 5816-42.

[12] Ahrens CD. Essentials of meteorology: an invitation to the atmosphere. 6th ed. Belmont, CA: Brooks/Cole 2011; p. 197.

[13] Girs AA. Macro-circulation method for long-term meteorological prognosis. Leningrad: Hydrometizdat Publ 1971; p. 480 (in Russian).

[14] Sidorenkov NS, Svirenko PI. Long-term fluctuations in atmospheric circulation. Sov Meteorol Hydrol 1983; 11: 12-5.

[15] Sidorenkov NS. The interaction between Earth's rotation and geophysical processes. Weinheim: Wiley-VCH Verla GmbH & Co. KGaA 2009; p.317.

[16] Metoffice UK. Available at: www.metoffice.gov.uk/hadobs/hadslp2 [Accessed: October 2012].

[17] NOAA_NCDC. Available at: ftp://ftp.ncdc.noaa.gov/pub/data/ghc n/blended/usingGHCNMv2/File: ncdc_blended_merg53v3b.dat.gz. [Accessed: 10 Dec 2009].

[18] Standish EM, Williams JC. Orbital ephemerides of the sun, moon and planets (PDF). Int Astron Union Comm 2010: 4: Ephemerides.

[19] Treloar NC. Luni-solar tidal influences on climate variability. Int J Climatol 2002; 22: 1527 - 42.

[20] Baart F, Pieter HA, van Gelder JM, de Ronde J, van Koningsveld M, Wouters B. The effect of the 18.6-year lunar nodal cycle on regional sea-level rise estimates, J Coast Res 2012; 28(2): 511-6.

[21] Chapront-Touzé M, Chapront J. Lunar tables and programs from 4000 B.C. to A.D. 8000. Richmond, Virginia: William–Bell 1991.

[22] The Australian BOM high quality temperature data sets. Available at: ftp://ftp.bom.gov.au/anon/home/ncc/www/change/HQdailyT. [Accessed: April 2010].

[23] DADisp 2002. Software program – DSP Development Corporation 2006. Available from: www.dadisp.com.